GEAP-3755
AEC RESEARCH AND
DEVELOPMENT REPORT
JUNE, 1963

ACCENT ON VALUE

BURNOUT CONDITIONS FOR NONUNIFORMLY HEATED ROD IN ANNULAR GEOMETRY, WATER AT 1000 PSIA

H_2O

By
E. JANSSEN
J. A. KERVINEN

U.S. ATOMIC ENERGY COMMISSION
CONTRACT AT(04-3)-189
PROJECT AGREEMENT 11

ATOMIC POWER EQUIPMENT DEPARTMENT
GENERAL ELECTRIC
SAN JOSE, CALIFORNIA

DISCLAIMER

GEAP-3755
AEC Research and
Development Report
June 1963

BURNOUT CONDITIONS FOR NONUNIFORMLY HEATED ROD IN ANNULAR GEOMETRY, WATER AT 1000 PSIA

by

E. Janssen
J. A. Kervinen

U. S. Atomic Energy Commission
Contract AT(04-3)-189
Project Agreement 11

Printed in U. S. A. [redacted]. Available from the
Office of Technical Services, Department of Commerce,
Washington 25, D. C.

ATOMIC POWER EQUIPMENT DEPARTMENT
GENERAL ELECTRIC
SAN JOSE, CALIFORNIA

TIO-1260

APPROVED:

D. H. Imhoff, Manager
Engineering Development

C. L. Howard
Project Engineer

ATOMIC POWER EQUIPMENT DEPARTMENT
GENERAL ELECTRIC
SAN JOSE, CALIFORNIA

EXTERNAL DISTRIBUTION LIST

	Number of Copies
William D. Manly Oak Ridge National Laboratory Oak Ridge, Tennessee	1
Mr. I. H. Mandil Assistant Director for Naval Reactors Division of Reactor Development Atomic Energy Commission Washington 25, D. C.	1
Westinghouse Electric Corporation Atomic Power Division Bettis Plant, Clairton Site P. O. Box 1526 Pittsburgh, Pennsylvania Attn: A. Squire	1
Mr. W. Cashin Knolls Atomic Power Laboratory P. O. Box 1072 Schenectady, New York	1
Robert Macheray Argonne National Laboratory Argonne, Illinois	1
F. W. Albaugh General Electric Company Hanford Works Hanford, Washington	1
Chief, Water Reactors Branch Civilian Reactors Division of Reactor Development U. S. Atomic Energy Commission Washington 25, D. C.	2
Mr. D. F. McElroy Northern States Power Company Minneapolis 2, Minnesota	1
Chief, Water System Project Branch Army Reactors Division of Reactor Development U. S. Atomic Energy Commission Washington 25, D. C.	1
Director, Reactor Program Division U. S. Atomic Energy Commission Chicago Operations Office 9700 South Cass Avenue Argonne, Illinois	3
Mr. J. M. West General Nuclear Engineering Corporation P. O. Box 245 Dunedin, Florida	1

	Number of Copies
Mr. W. H. Zinn Combustion Engineering Incorporated Nuclear Division Prospect Hill Road Windsor, Connecticut	1
Dr. W. E. Shoupp Westinghouse Electric Corporation Atomic Power Department P. O. Box 355 Pittsburgh 30, Pennsylvania	1
Mr. C. B. Graham Allis-Chalmers Manufacturing Company Atomic Energy Division Milwaukee 1, Wisconsin	1
H. Etherington Allis-Chalmers Manufacturing Company Nuclear Power Department P. O. Box 8697 Washington 11, D. C.	1
A. Bethel Consumers Power Company 212 West Michigan Avenue Jackson, Michigan	1
Senior USAEC Representative U. S. Mission to the European Communities c/o U. S. Embassy Brussels, Belgium	1
Dr. Stanley A. Szawlewicz, Chief Reactor Safety Branch Division of Reactor Development U. S. Atomic Energy Commission Washington 25, D. C.	1
Dr. Warren E. Nyer SPERT Project Manager Phillips Petroleum Company P. O. Box 1259 Idaho Falls, Idaho	1
J. F. O'Brien Mail No. W-179 Martin Company, Nuclear Division Middle Row, Maryland	1

LEGAL NOTICE

TABLE OF CONTENTS

LIST OF ILLUSTRATIONS

SUMMARY

Tests were run at the General Electric Company, Atomic Power Equipment Department, to determine the burnout conditions for a non-uniformly heated rod in an annular geometry. Two special electrically heated rods were used; the cosine rod, which gave an approximate cosine axial heat flux distribution; and the truncated cosine rod, identical to the cosine, except for one end having been cut short. The rod to be tested was placed in a circular tube test section to form the annular flow path for the water coolant. Only the rod was heated; the outer surface (tube) was essentially adiabatic. Orientation was vertical, with flow upward. The tests were run at the following conditions:

Rod OD:	0.540 inch
Tube ID:	0.875 inch
Hydraulic diameter:	0.335 inch
Heated length, cosine rod:	108 inches
truncated cosine:	91 inches
Pressure:	1000 psia
Flow rate:	0.84×10^6 to 1.40×10^6 lb/hr-ft^2
Steam quality at exit:	12 to 35 percent

For each flow and inlet subcooling, the electrical power was increased until burnout was reached, thus establishing a burnout condition. Each nonuniform rod was instrumented with thermocouples in the region of anticipated burnout. The local heat flux and local quality at each position at which a thermocouple indicated a temperature rise, were determined for each burnout run.

The local heat flux at burnout was plotted versus the local quality at burnout, for the two non-uniform rods. The uniform rod burnout correlation from Reference 6 was superposed for comparison. The nonuniform rod data points averaged from 9 to 20 percent low. The magnitude of this deviation is considered small, and of the same order as that for the uniform rod data upon which the correlation was originally based. It is concluded that the uniform rod burnout correlation can be used to predict burnout for cosine heat flux distribution. It is tacit in this conclusion that burnout depends only on local conditions of quality and flow. A method for predicting burnout for a nonuniform heat flux distribution is developed and applied to all the cosine and truncated cosine rod data. The predicted average heat flux at burnout is within +11 percent, -2-1/2 percent of the measured average heat flux. The method (1) predicts the most probable position at which burnout will occur, and (2) accurately predicts the power level at which burnout will occur.

INTRODUCTION

In the boiling water-type reactor, light water under high pressure flows upward through the core channels to cool the fuel rods. Boiling takes place at the fuel-water interface, and net steam is produced at the core exit. If the heat flux is raised, the outside surface temperature of the fuel rod may change slightly, but remains just a few degrees above saturation until a critical value of the heat flux is reached. Past this point, the temperature starts to rise rapidly, attended by oscillations. The rate of rise, and the amplitude of oscillation, depend upon the conditions, i. e., quality (enthalpy) and mass velocity of the bulk coolant at the position of burnout. In general, the lower the quality, the more abrupt is the temperature rise.

"Burnout", as commonly used, applies to the critical point* past which the surface temperature starts to rise rapidly. It will be so used in this report, even though this is a misleading usage under conditions where material failure does not occur at heat fluxes past the critical point. The currently accepted practice in boiling water reactor design is to limit the design heat flux to a fraction of the burnout heat flux.

In the past, the conditions for burnout have generally been determined using channels in which the distribution of power to the heat transfer surface is uniform. The question may properly be raised whether the conditions so determined apply to the heat transfer surfaces in a reactor core, where the power distribution is not uniform. Rather, for a given channel, it is some function of y, where y is distance along the vertical axis of the core. The cosine, taking the origin of y at the core center, is commonly used to approximate this power distribution function.

Some effort has been expended to answer the question posed above, whether burnout conditions determined for a uniform heat flux distribution apply to cases where the heat flux distribution is not uniform. DeBortoli, Roarty, and Weiss, [1] and Weiss, [2] measured burnout conditions for non-uniform distributions along a rectangular channel. Galson and Polomik, [3] measured burnout conditions for a non-uniform distribution along an internally heated annulus. Styrikovich, Miropol'skii and Chzhao-Yuan Shen, [4] and Swenson, Carver, and Kakarala, [5] measured burnout conditions for non-uniform distribution along circular tubes.

The authors of Reference 1 found that for a cosine axial heat flux distribution, the conditions at the position of burnout were bounded by two earlier correlations based on uniform heat flux data. The authors of Reference 3 found that, again for a cosine heat flux distribution, the heat flux in the region of burnout was low relative to uniform heat flux results. The findings of the other authors, for various forms of heat flux distribution, suggest that the burnout heat flux may be lowered if

*This critical point is also referred to as the "departure from nucleate boiling" (DNB) and as the boiling "crisis".

the heat flux ahead of the region of burnout is higher than the heat flux in the burnout region. However, the total amount of non-uniform heat flux data obtained by all of these investigators is small, and there is some uncertainty about their test conditions. It is therefore felt that, even for the geometries tested, their results are not conclusive.

About 3 years ago, the General Electric Company's Atomic Power Equipment Department (APED), as part of the Fuel Cycle Program, set out to determine the burnout conditions for a single rod with non-uniform axial heat flux distribution, in an annular type geometry. This work was carried on in parallel with the uniformly heated single rod work, described in another report. [6]

The work done at APED and reported here, had as its objectives:

1. To measure the burnout conditions for an internally heated annular geometry for which the axial heat flux distribution is approximately a cosine.
2. To compare the measured burnout conditions with burnout conditions for a uniform heat flux distribution. [6]
3. To establish a procedure by means of which the burnout conditions for a cosine distribution can be reliably predicted from uniform distribution results.

The report of the work follows.

EQUIPMENT AND PROCEDURE

All of the APED single rod burnout data were obtained using an electrically heated rod placed inside a circular tube test section, thus forming an annular flow path for the water. The tube surface, i.e., the outer surface of the annulus, was unheated.

The nonuniformly heated rods were tested under a series of conditions of flow and inlet enthalpy, simulating those which might occur in a reactor core. For each condition, the electrical power was increased until burnout was reached, thus establishing a burnout condition.

The equipment used to accomplish this simulation for nonuniform power distribution is the same (except for the rods themselves) as that used for the uniform single rod work, and is described in detail in Reference 6. A brief description of rods and equipment is given here.

Cosine and Truncated Cosine Rods

The heated portion of each electrically heated rod was a section of stainless steel tube. Copper extensions (electrodes) with the same OD were silver soldered to the ends. Thermocouples were passed through one of the electrodes and attached, by a spot welding technique, to the inside surface of the stainless steel tube. A typical assembled rod is shown in Figure 1.

To investigate burnout under nonuniform heat flux distribution, six special rods were prepared. The external dimensions of these rods were the same as for the 0.540-inch diameter uniform rods described in Reference 6, but the heat flux was caused to vary in the axial direction by intentionally making the wall thickness vary, the relative heat flux varying approximately inversely as the wall thickness.

It was intended that the heat flux have approximately a cosine distribution, hence the name "cosine" was assigned to the rods. However, there is an inflection in the curve of relative heat flux ψ near both ends for the first three rods tested, as shown in Figure 2A. Past the point of inflection ψ is no longer approximated by a cosine.

Seventeen inches were cut off the remaining three cosine rods, to eliminate the inflection at the exit end. These particular rods are referred to hereinafter as the truncated cosine rods. The relative heat flux distribution for these three rods is shown in Figure 2B. ψ along the exit half is approximated by a cosine up to the end of the rod.

Table 1 gives the variation of resistance with length for all six rods, as measured at room temperature. The curves ψ vs. y, of Figures 2A and 2B, are based on the measured values of Table 1.

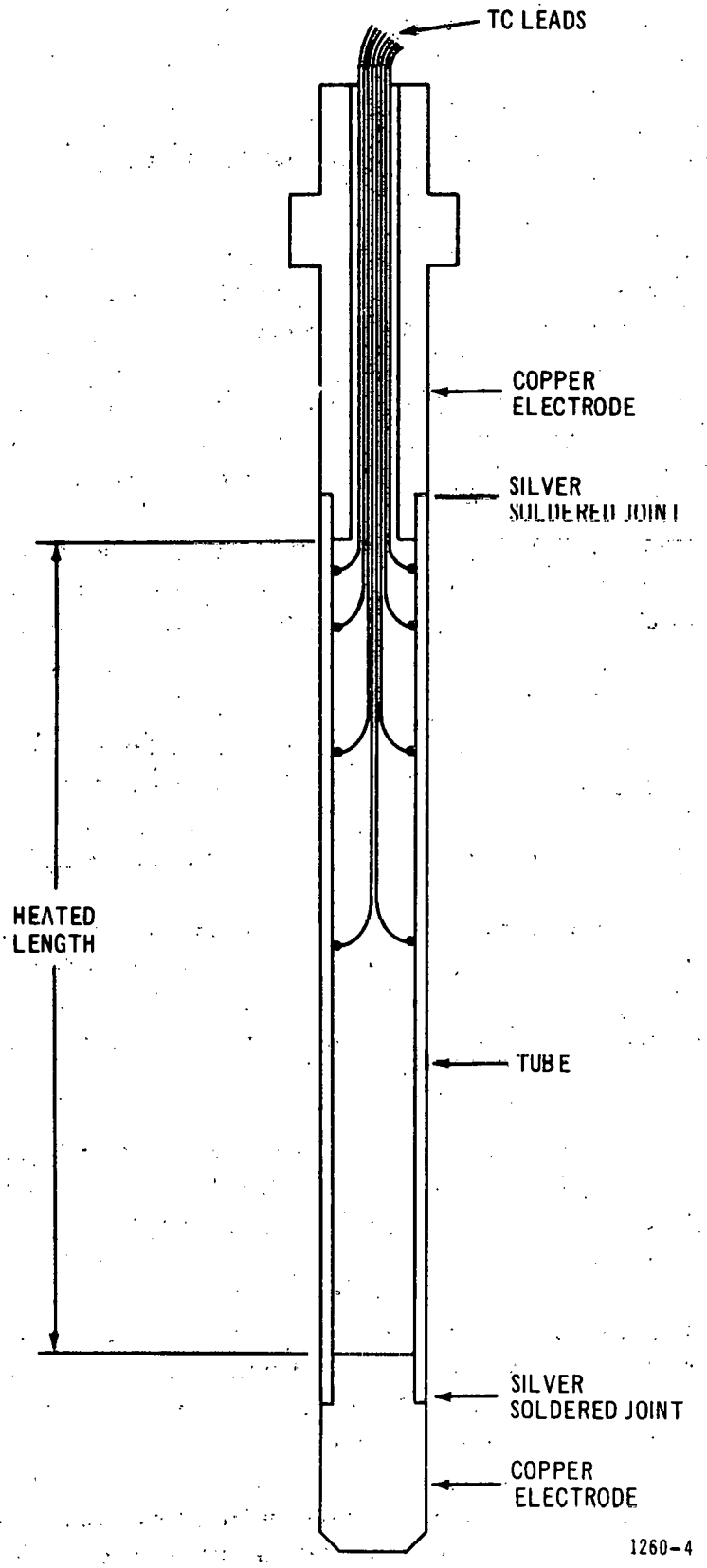

Figure 1. Typical Assembled Rod

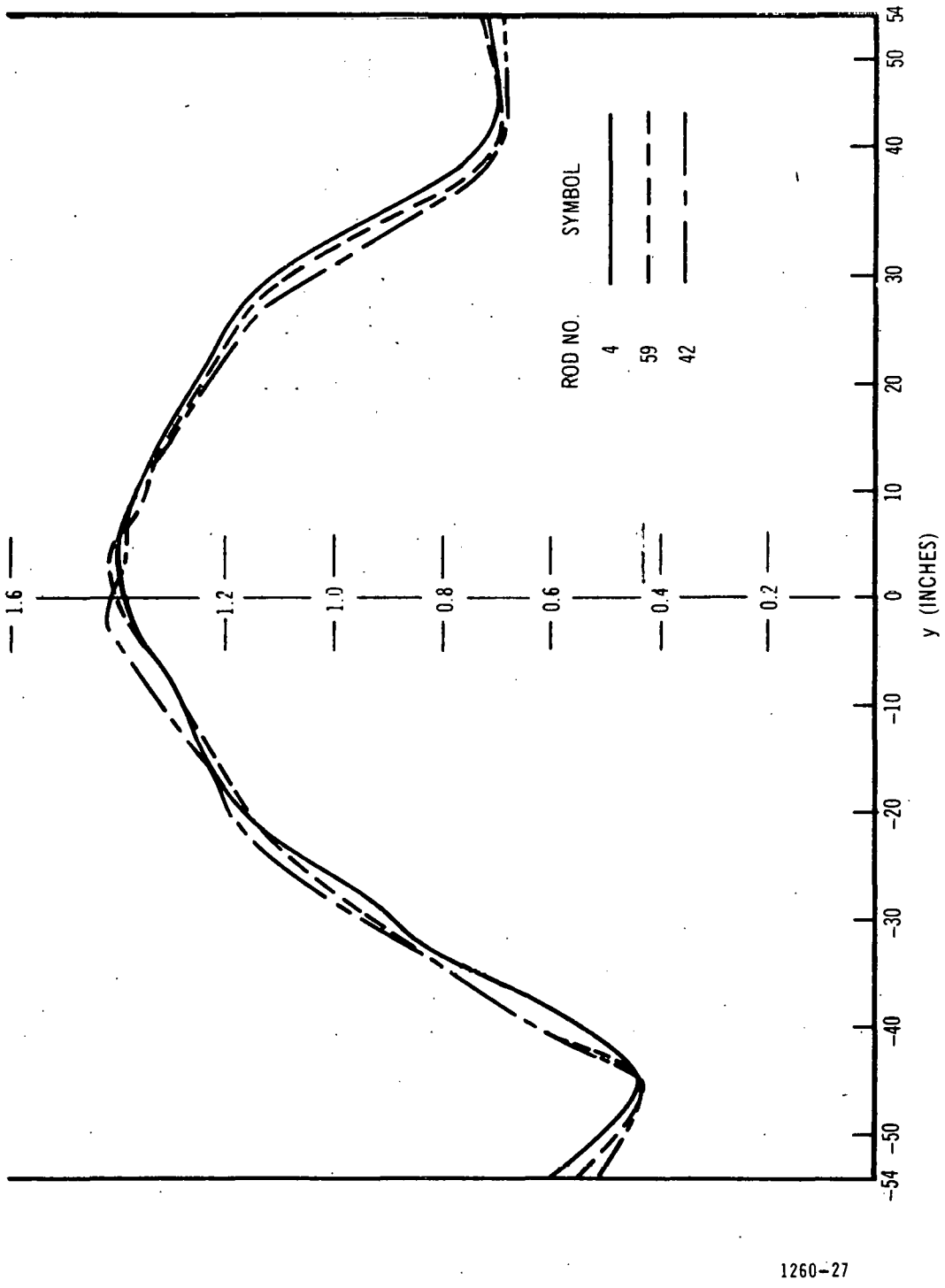

Figure 2A. Relative Heat Flux Distribution - Cosine Rod

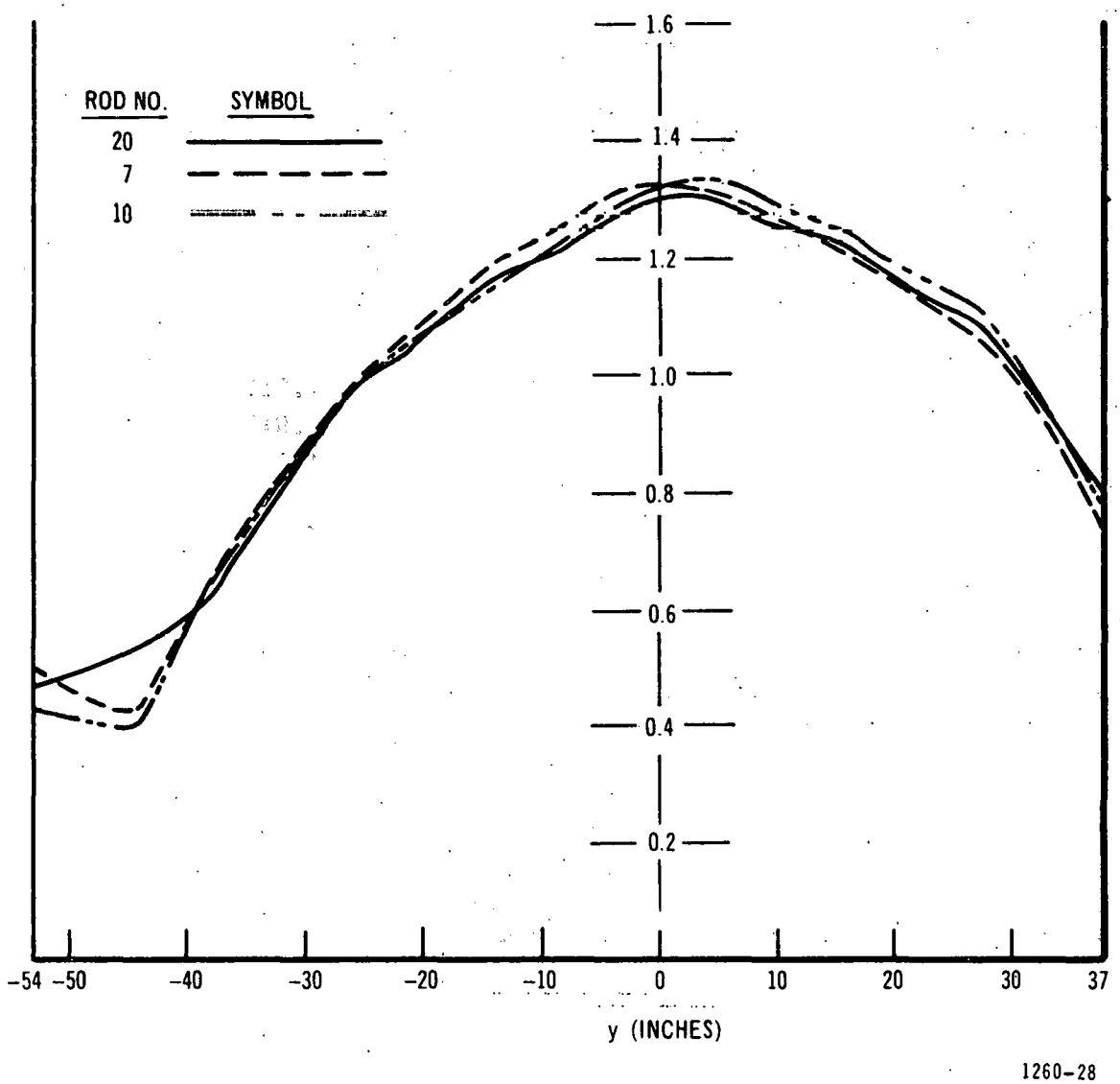

Figure 2B. Relative Heat Flux Distribution - Truncated Cosine Rod

TABLE 1

COSINE AND TRUNCATED COSINE ROD RESISTANCE*

	Rod No. 4 347 Stainless			Rod No. 59 347 Stainless			Rod No. 42 Incoloy		
y (in.)	r (ohms)	r/R	ψ**	r (ohms)	r/R	ψ**	r (ohms)	r/R	ψ**
-54	0	0	0.528	0	0	0.496	0	0	0.475
-48	0.00096	0.294	0.424	0.00089	0.0276	0.429	0.00117	0.0264	0.422
-42	0.00173	0.0529	0.561	0.00166	0.0514	0.658	0.00222	0.0499	0.654
-36	0.00275	0.0841	0.815	0.00285	0.0879	0.831	0.00383	0.0862	0.841
-30	0.00423	0.1294	0.952	0.00434	0.1341	1.008	0.00590	0.1330	1.040
-24	0.00596	0.1823	1.150	0.00616	0.1901	1.148	0.00847	0.1907	1.170
-18	0.00805	0.2462	1.233	0.00822	0.2539	1.220	0.01136	0.2558	1.235
-12	0.01029	0.3147	1.272	0.01042	0.3217	1.276	0.01440	0.3244	1.329
-6	0.01260	0.3853	1.360	0.01271	0.3926	1.370	0.01768	0.3982	1.410
-0	0.01507	0.4609	1.393	0.01518	0.4687	1.410	0.02116	0.4765	1.381
6	0.01760	0.5382	1.371	0.01771	0.5471	1.349	0.02457	0.5533	1.377
12	0.02009	0.6144	1.313	0.02014	0.6220	1.301	0.02797	0.6298	1.292
18	0.02248	0.6873	1.237	0.02248	0.6943	1.228	0.03115	0.7016	1.210
24	0.02472	0.7561	1.174	0.02469	0.7625	1.152	0.03414	0.7688	1.136
30	0.02686	0.8213	1.014	0.02676	0.8265	0.975	0.03694	0.8319	0.932
36	0.02870	0.8776	0.793	0.02851	0.8806	0.751	0.03924	0.8837	0.724
42	0.03014	0.9217	0.700	0.02986	0.9223	0.694	0.04102	0.9239	0.681
48	0.03141	0.9606	0.709	0.03111	0.9609	0.704	0.04270	0.9617	0.690
54	0.03270	1.0000		0.032377	1.0000		0.04441	1.0000	

* All values in this table are based on resistance measurements at room temperature.

** $\psi = \dfrac{dr/dy}{R/L}$

TABLE 1 (Continued)

	Rod No. 20 347 Stainless			Rod No. 7 347 Stainless			Rod No. 18 347 Stainless		
y (in.)	r (ohms)	r/R	ψ**	r (ohms)	r/R	ψ**	r (ohms)	r/R	ψ**
-54	0	0	0.481	0	0	0.459	0	0	0.417
-48	0.00093	0.0317	0.538	0.00088	0.0303	0.428	0.00079	0.0275	0.401
-42	0.00197	0.0672	0.626	0.00170	0.0585	0.637	0.00155	0.0539	0.633
-36	0.00318	0.1085	0.797	0.00292	0.1005	0.809	0.00275	0.0957	0.802
-30	0.00472	0.1610	0.978	0.00447	0.1539	0.982	0.00427	0.1485	0.981
-24	0.00661	0.2254	1.066	0.00635	0.2186	1.081	0.00613	0.2132	1.076
-18	0.00867	0.2957	1.159	0.00842	0.2898	1.185	0.00817	0.2842	1.155
-12	0.01091	0.3721	1.216	0.01069	0.3680	1.248	0.01036	0.3604	1.229
-6	0.01326	0.4522	1.288	0.01308	0.4503	1.331	0.01269	0.4414	1.308
0	0.01575	0.5372	1.304	0.01563	0.5380	1.316	0.01517	0.5277	1.340
6	0.01827	0.6231	1.252	0.01815	0.6248	1.269	0.01771	0.6160	1.282
12	0.02069	0.7057	1.218	0.02058	0.7084	1.209	0.02014	0.7005	1.238
18	0.02304	0.7858	1.135	0.02290	0.7883	1.142	0.02249	0.7823	1.166
24	0.02524	0.8608	1.078	0.02508	0.8633	1.061	0.02470	0.8591	1.099
30	0.02732	0.9318	0.905	0.02712	0.9336	0.889	0.02678	0.9315	0.918
36	0.02907	0.9915		0.02882	0.9921		0.02852	0.9920	
37	0.02932	1.0000	0.785	0.02905	1.0000	0.743	0.02875	1.0000	0.775

* All values in this table are based on resistance measurements at room temperature.

** $\psi = \frac{dr/dy}{R/L}$

Under test conditions, the temperature of the rods was, of course, considerably above room temperature. However, the function ψ is not affected by the temperature level, but only by the presence of axial temperature gradients. It can be shown that:

1. Even under the combination of test conditions most likely to produce axial temperature gradients (high flow, high inlet subcooling, and low average heat flux), the rod surface temperature at the inlet end was at saturation. Thus, the surface temperature was essentially constant for all runs.
2. If the surface temperature is constant, the average radial temperature is very nearly constant. The greatest axial variation in average radial temperature would occur at the highest average heat flux (Run No. 20). This was calculated to be 16 F, which would cause a negligible change in local resistivity. Therefore, any change in ψ from its value at room temperature was negligible.

It will be noted by reference to Table 1 that the material for the cosine rods was either 347 stainless steel or Incoloy. This is in contrast to the uniform rods, which were, in general, of 304 stainless steel. However, no difference in burnout due to material differences is believed to exist between 304, 347, and Incoloy. This is supported by the conclusion reported in Reference 7, based on burnout data with Nickel. Zircaloy-2 (29 microinches and 120 microinches roughness), and 304 stainless steel.

The cosine rods were assembled in essentially the same manner as the uniform rods (see Figure 1). The location of the thermocouples for the cosine rods was different than for the uniform rods. The location for the cosine rods is given in Table 4 (see Results and Discussion).

Test Section

Two test sections were used. The first was in existence at the start of the program described in this report, and is referred to hereinafter as the old test section. The second was built after the start of this program, and is referred to hereinafter as the new test section.

The old test section is shown in Figure 3. It has a fixed ID of 0.875 inch. The rod is held concentric in the tube by sapphire spacer pins. The spacer pins are arranged in groups of three (see detail, Figure 3). The groups are spaced 24 inches apart along the axis. In addition, there are single sapphire pins located halfway between adjacent groups. These single pins are all in a line, on one side of the test section. There are plenum chambers at both the inlet (bottom) and exit (top) ends of the test section. A sheathed thermocouple is inserted into the flow at the inlet end for measurement of inlet temperature. This, plus system pressure, define the inlet conditions.

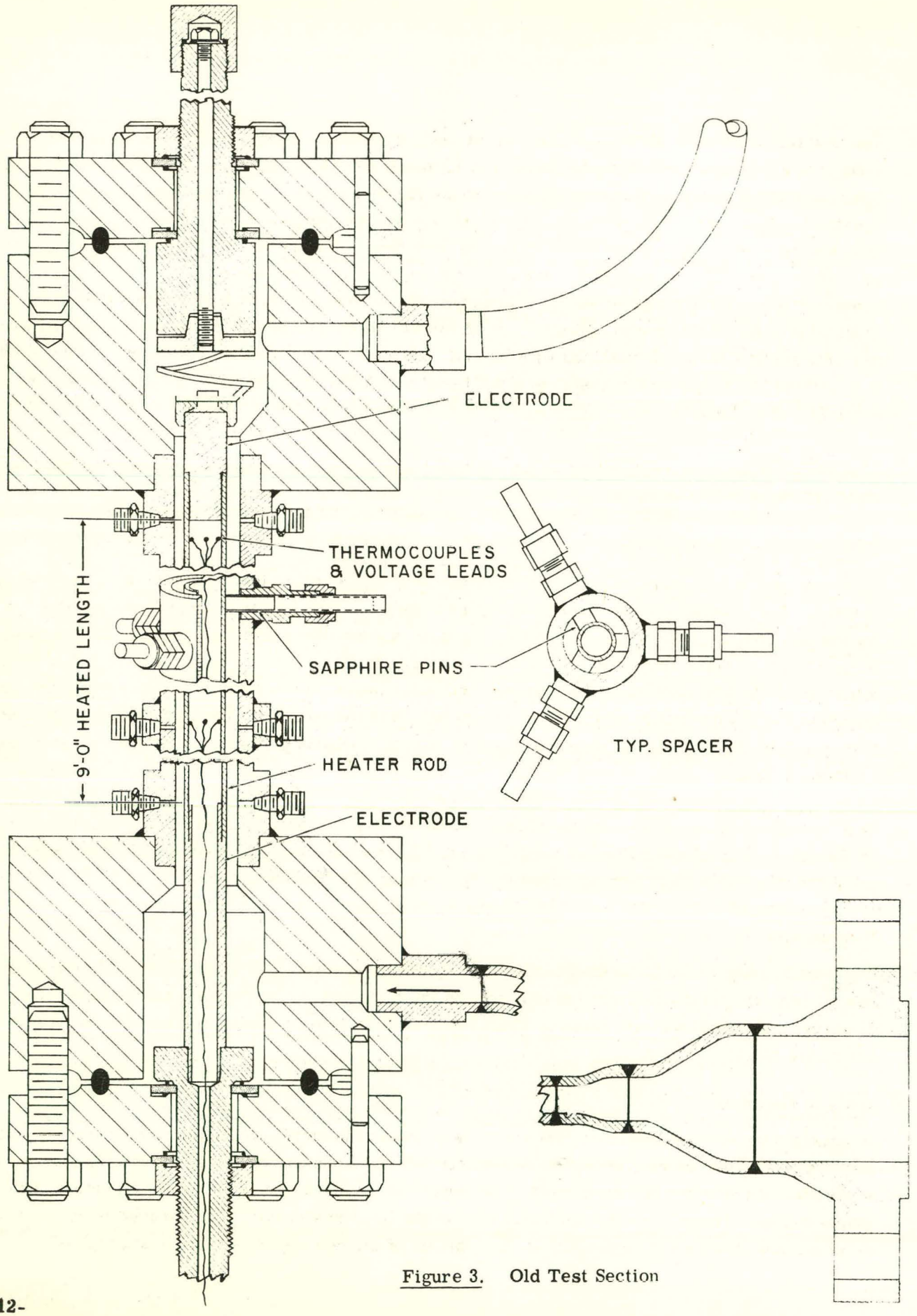

Figure 3. Old Test Section

The new test section is shown in Figure 4. It has a removable liner which permits varying the ID. However, for all the tests reported here, the ID was 0.875 inch, the same as for the old test section. There are other minor differences relative to the old test section. The spacer pins are of Rulon sheathed in stainless steel, with an unsheathed segment for insulating purposes. The new spacer pins are arranged in groups of three as before (see detail, Figure 4), but the groups are spaced on 18-inch instead of 24-inch centers, and there are no single intermediate pins. There are two thermocouples at the inlet end instead of one. However, it has been shown in Reference 6 (see Figure 18A of Reference 6), that there is essentially no difference between the burnout results obtained with the new test section and those obtained with the old, when the test conditions are otherwise the same. It may be concluded that for the tests reported here, any differences between the old and the new test sections are negligible.

The three cosine rods were tested in the old test section. The three truncated cosine rods were tested in the new test section.

Heat Transfer Facility Loop

The test section was installed in the APED Heat Transfer Facility loop, with the flow vertical and upward. The general arrangement is shown in Figure 5. The loop is equipped with a pump for forced circulation, a valve for controlling the flow, a subcooler for controlling the test section inlet temperature, a riser above the test section, a steam drum, a finned condenser which functions as a heat sink (the test section is the heat source), and a louver arrangement for controlling the rate of condensation (by controlling the rate of cooling air over the outside of the condenser). The louvers are controlled by a pressure responsive servo, which functions to hold the system pressure constant to within $\pm$ 10 psia.

Demineralized water is used exclusively in the loop. Conductivity is used as the measure of quality of the water, and is maintained at better than 0.2 microohm-cm. Analysis of the water after operating the loop for a short period shows 0.1 to 0.4 ppm of dissolved oxygen.

Instruments

The loop is suitably instrumented to measure system pressure, flow rate, electrical power to the heated rod, and temperature at the test section inlet, as well as other less critical quantities. The more critical quantities are listed in Table 2 below, with type of measuring instrument, and with estimated limits of error.

Burnout Detection

In approaching the burnout point, the power is increased in small but finite steps of from one to two percent of the total power. Detection of burnout depends upon having gone past the burnout point by something of the order of one percent, whereupon the temperature of the affected portion of the rod starts to rise. There is a corresponding rise in the local resistivity. The burnout detection device detects small changes in resistance in that portion of the rod where burnout is anticipated.

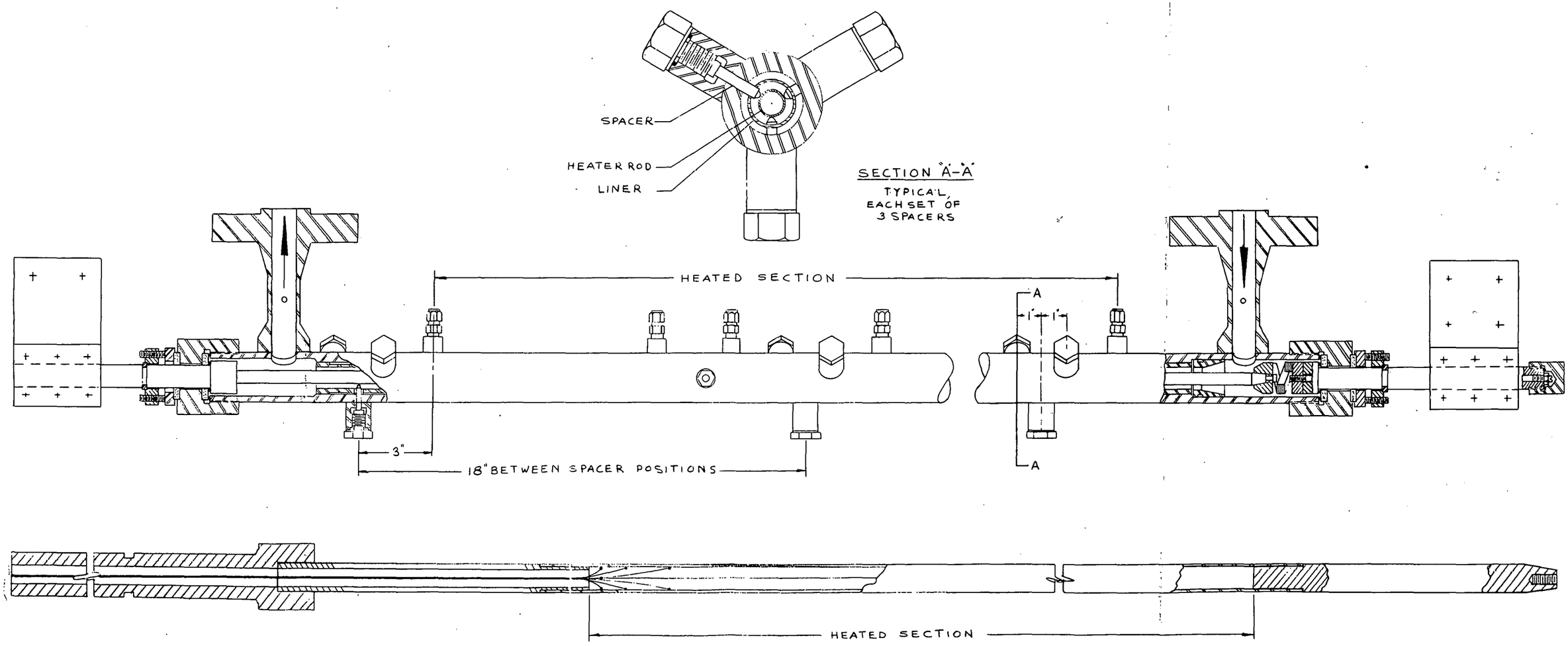

Figure 4. New Test Section

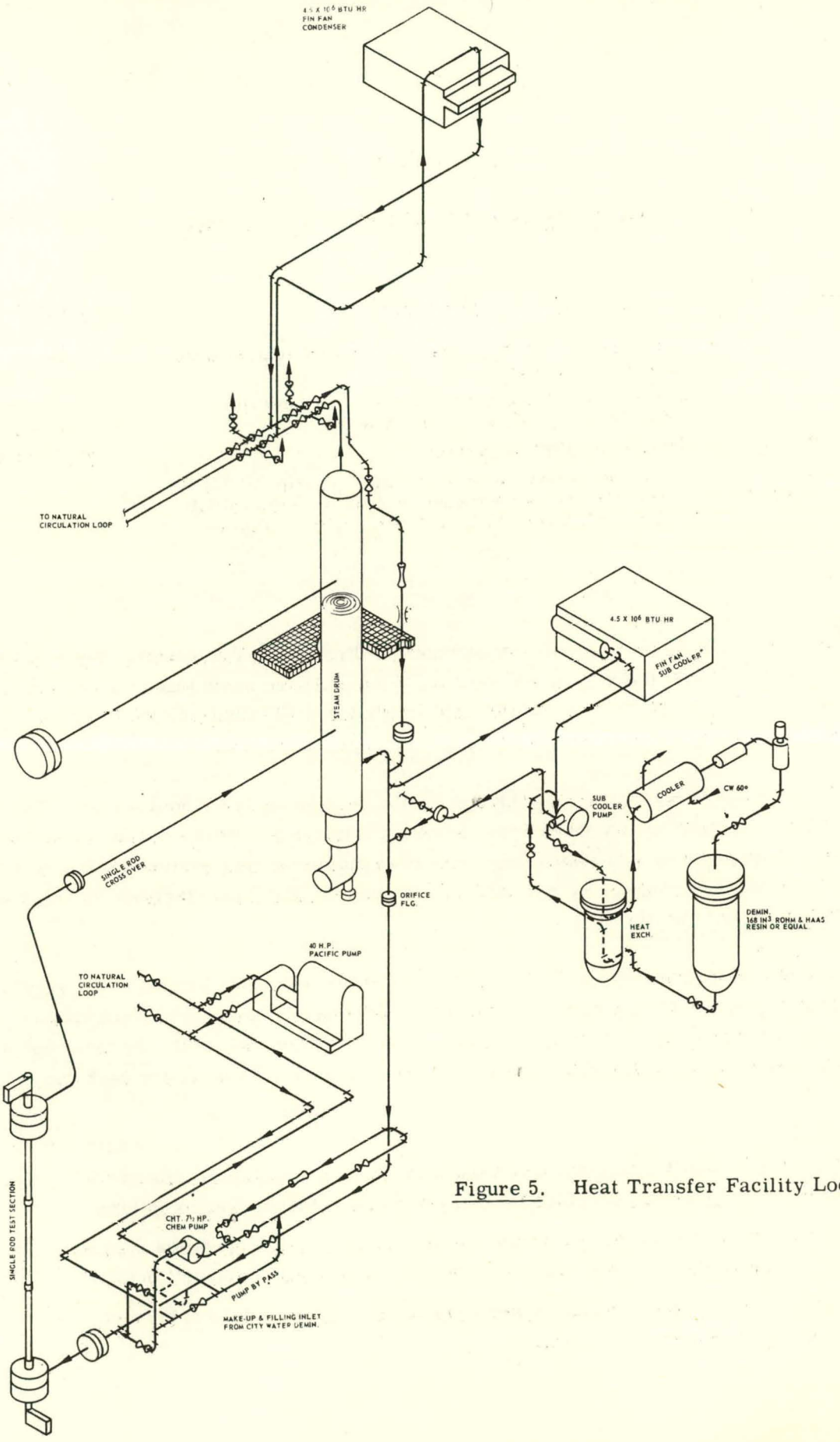

Figure 5. Heat Transfer Facility Loop

TABLE 2

LOOP INSTRUMENTS AND LIMITS OF ERROR

Quantity	Instrument	Limits of Error
System Pressure	Heise gage, bourdon type, calibrated against dead weights and piston.	± 5 psi
Mass Rate	Orifice and 60-inch manometer. Temperature measured at orifice and manometer.	± 2 percent (less at high flows)
Electrical Power	Recording Kilowatt meter	± 3 percent
Test Section Inlet Temperature	Calibrated thermocouple, "cold" junction at 150 F ±1 F, millivolts recorded with Brown Multipoint, occasional check with slide wire potentiometer.	± 3 F

A schematic circuit of the burnout detector is shown in Figure 6. Two adjacent segments of the rod (one of which includes the anticipated location of burnout) are made legs of a resistance bridge. A rise in average resistance in one of the segments produces an imbalance in the bridge. The resulting signal trips out the electrical power and indicates a burnout.

There must be three voltage taps along the rod for the requirements of the detector. Two or three of the thermocouples with which each of the rods was instrumented were used for these taps. If a thermocouple is being used as a voltage tap, it is unavailable for temperature measurement. The location of all the thermocouples is given in Table 3, and the particular thermocouples in use as voltage taps are noted for each run.

The detection device described above is backed up with thermocouples located in the region where burnout is anticipated. A temperature rise was indicated by one or more of these thermocouples for all but two of the runs (see Results and Discussion). The location of the thermocouples in use, and the particular thermocouples indicating a temperature rise, are noted for each run in Table 3.

Test Procedure

The combinations of heat flux distribution and flow parameters which were tested for burnout are listed in Table 4. The testing procedure for any given combination was as follows:

1. Supply electrical power to the test section until a quasi-steady condition is reached, whereby the steam drum contains both steam and water, in thermodynamic equilibrium.
2. Adjust the louver servo to regulate system pressure at the desired value (1000 psia for all the cosine and truncated cosine runs).

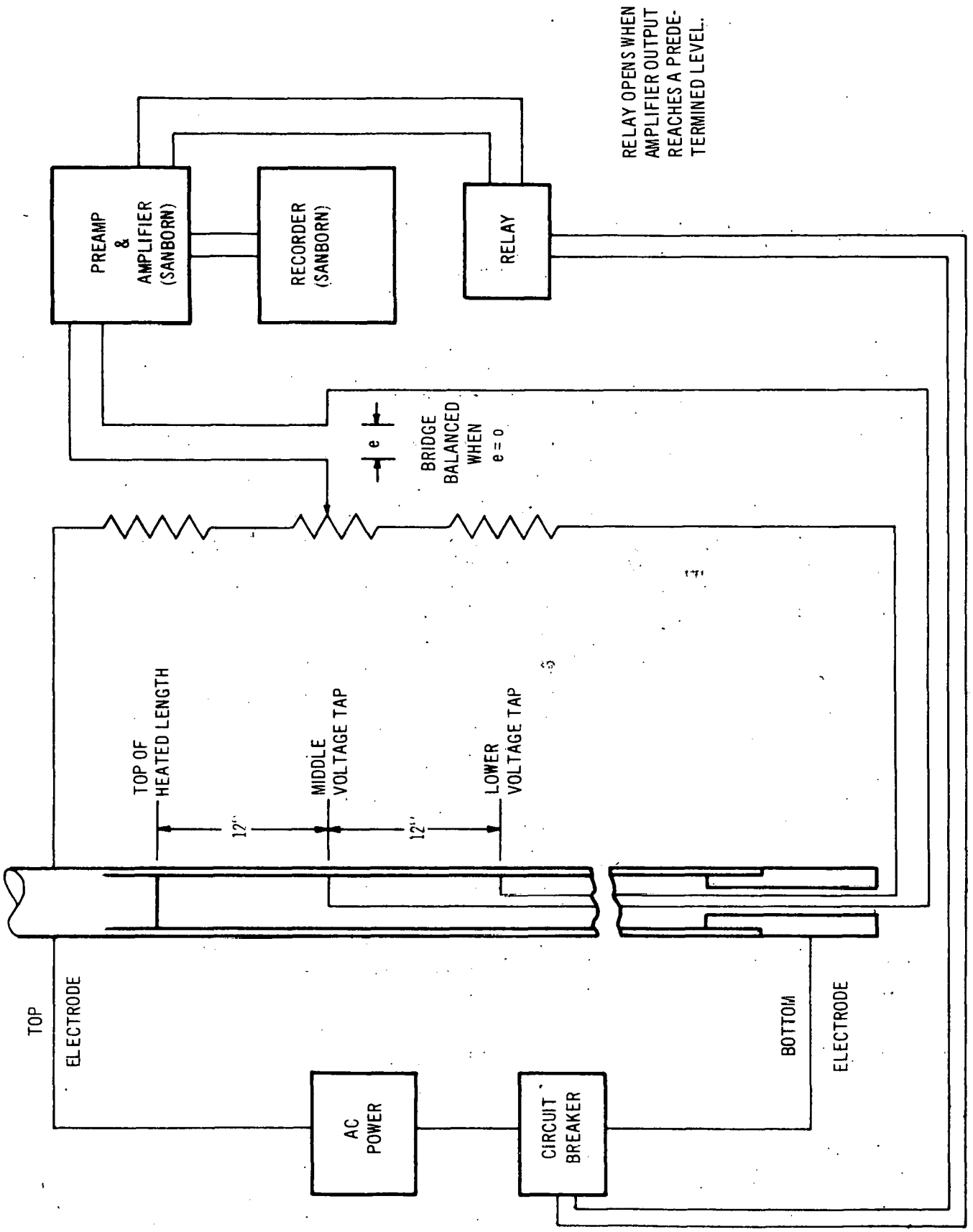

Figure 6. Schematic Circuit of Burnout Detection Device

TABLE 3

THERMOCOUPLES

S - Thermocouple connected to Sanborn recorder.

V - Thermocouple used for voltage tap. (The voltage tap nearest the exit end was moved to the top electrode after run C-25; hence only two thermocouples were needed for voltage taps for all subsequent runs.)

Run No.	Rod No.	Thermocouple Number/Location (Inches)									
		1 53.5	2 49.5	3 44	4 39.5	5 35	6 30.5	7 26	8 21.5	9 17	
C-1	4			S*	V		S	V		V	
		1 52	2 49	3 46	4 43	6 37	7 34	8 31	9 28	10 25	14 13
C-2	59	S		V	S	S	S*	S	V	S	V
C-3	59	S		V	S*	S	S*	S	V	S	V
C-4	59	S		V	S*	S	S*	S	V	S	V
C-5	59	S		V	S*	S	S*	S	V	S	V
C-6	59	S		V	S	S	S*	S	V	S	V
C-7	59	S	V		S	S	S*	S	V	S	V
C-8	59	S	V		S	S	S*	S	V	S	V
C-9	59	S	V		S	S	S*	S	V	S	V
C-10	59	S	V		S	S	S*	S	V	S	V
C-11	59	S	V		S	S	S*	S	V	S	V
C-12	59	S	V		S	S	S*	S	V	S	V
C-13	59	S	V		S	S	S*	S	V	S	V
C-14	59	S	V		S	S	S*	S	V	S	V
C-15	59	S	V		S	S	S*	S	V	S	V
C-16	59	S	V		S	S	S*	S	V	S	V
C-17	59	S	V		S	S	S*	S	V	S	V
C-18	59	S	V		S	S	S*	S	V	S	V
C-19	59	S	V		S	S*	S*	S	V	S	V
C-20	59	S	V		S	S	S	S	V	S*	V
C-21	42	V	S*		S	S	S	S	V	S	V
C-22	42	V	S*		S	S	S	S	V	S	V
C-23	42	V	S*		S	S	S	S	V	S*	V
C-24	42	V	S*		S	S	S	S	V	S	V
C-25	42	V	S		S	S	S	S	V	S	V

*Traces for these thermocouples indicate temperature rise at burnout.

TABLE 3 (Continued)

Run No.	Rod No.	Thermocouple Number/Location (Inches)													
		1 36.6	2 35	3 33	4 31	5 29	6 27	7 25	8 23	9 21	10 19	11 16	12 13	13 10	14 7
C-26	20	S			S*		S	V		S			V	S	
C-27	20	S			S*		S	V		S			V	S	
C-28	20	S			S*		S	V		S			V	S	
C-29	20	S			S*		S	V		S			V	S	
C-30	20	S	S	S	S	S*		V					V		
C-31	7	S		S		S	S	S	V					V	
C-32	7	S*		S*	S*	S*	S*		V					V	
C-33	7	S		S	S*	S	S		V					V	
C-34	7			S	S*	S	S		V		S			V	
C-35	7			S*	S*	S*	S*		V		S*			V	
C-36	7			S	S*	S	S		V		S			V	
C-37	18	S		S*	S*	S*	S		V					V	
C-38	18	S		S*	S*	S	S		V					V	
C-39	18	S		S*	S*	S	S		V					V	
C-40	18	S		S*	S*	S	S		V					V	
C-41	18	S		S*	S*	S	S		V					V	
C-42	18	S		S*	S*	S	S		V					V	
C-43	18	S*		S*	S	S	S		V					V	
C-44	18	S*		S*	S*	S	S		V					V	
C-45	18	S		S*	S	S	S		V					V	
C-46	18	S		S*	S*	S	S		V					V	
C-47	18	S		S	S*	S	S		V					V	
C-48	18	S		S	S*	S*	S		V					V	

3. Set the flow at some predetermined value and manually regulate the flow to hold this value constant.
4. Adjust the subcooler to give approximately the desired value of inlet subcooling.
5. Bring up the electrical power slowly until a burnout is indicated. The pressure, flow, power, and inlet subcooling which exist at the time of burnout indication constitute the data for a burnout point.
6. The subcooling is changed to a new value and step 5 is repeated.
7. Steps 5 and 6 are repeated several times until the burnout characteristics for the given rod and flow are adequately defined.

TABLE 4

COSINE ROD PARAMETER COMBINATIONS

Concentric Annular Channel

D_1 = Rod diameter; D_h = Hydraulic diameter; D_2 = Tube (liner) diameter; L = Heated length

Comb. No.	D_1 (in.)	D_2 (in.)	D_h (in.)	L (in.)	P (psia)	$G/10^6$ (lb/hr-ft^2)	Special Features (O = Old Test Section N = New Test Section)
1	0.540	0.875	0.335	108	1000	0.84	O; cosine rod
2						1.12	O; cosine rod
3						1.40	O; cosine rod
4	0.540	0.875	0.335	91	1000	0.84	N; truncated cosine rod
5						1.12	N; truncated cosine rod
6						1.40	N; truncated cosine rod

EQUATIONS FOR REDUCING THE DATA; UNIFORM ROD BURNOUT CORRELATION

The first step in reducing the data is to determine the average heat flux at burnout $\overline{\phi}_{bo}$ in terms of the quality x_e (i. e., enthalpy) at test section exit, and the mass rate per unit area G. It is necessary to calculate G, $\overline{\phi}_{bo}$, and x_e from the recorded data.

The form of the recorded data before reduction is as follows:

1. Pressure, psig.
2. Orifice temperature, millivolts, chromel-alumel thermocouple.
3. Test section inlet temperature, millivolts, chromel-alumel thermocouple.
4. Flow, inches manometer deflection.
5. Room temperature, °F
6. Power, kilowatts

The pressure is converted to absolute pressure, P, by simply adding 15 psi to the Heise gage reading.

The orifice and test section inlet thermocouple readings are converted to degrees Farenheit by reference to a chart. The orifice and test section inlet temperatures are T_{13} and T_1, respectively.

The mass rate of flow is determined from the following relationships:

$$\frac{\dot{W}}{k} = w A_o \sqrt{2g\Delta h}, \quad \text{lb/sec} \tag{1}$$

w = density of water at temperature T_{13}, lb/ft^3
(The steam table value for saturated liquid is used.)

$$A_o = A_{o-75} \left\{ 1 + 2 \alpha (T_{13} - 75) \right\}, \quad ft^2 \tag{2}$$

A_{o-75} = Orifice area at 75 F, ft^2

α = linear coefficient of expansion for 304 stainless steel (both the orifice plate and flanges are of this material).

$g = 32.17 \text{ ft/sec}^2$

$$\Delta h = \frac{w_r}{w} \left[\left(\frac{w_{man}}{w_r} - 1 \right) \frac{\Delta h'}{12} - \Delta z \left(1 - \frac{w}{w_r} \right) \right], \quad \text{ft} \tag{3}$$

w_r = density of water at room temperature T_r, lb/ft^3

w_{man} = density of manometer fluid at room temperature T_r, lb/ft^3

$\Delta h'$ = manometer deflection, inches

Δz = elevation of upstream orifice tap minus elevation of downstream orifice tap, ft.

k = orifice discharge coefficient, which can be specified in terms of $\frac{N_R}{k}$

$$\frac{N_R}{k} = \frac{\dot{W}}{k} \frac{D_o}{A_o} \frac{1}{\mu} \tag{4}$$

D_o = orifice diameter, ft.

μ = viscosity of water at temperature T_{13}, lb/sec-ft

The total flow rate is obtained from

$$\dot{W} = k \left(\frac{\dot{W}}{k} \right) \tag{5}$$

and the flow rate per unit area is given by

$$G = \frac{\dot{W}}{A} \tag{6}$$

where A is the cross sectional area of flow.

The electrical power is converted to equivalent thermal units:

$$q = 0.9475 \times (\text{kilowatts}), \text{ Btu/sec} \tag{7}$$

The average heat flux $\bar{\phi}$ is the thermal energy rate divided by the heat transfer area.

$$\bar{\phi} = \frac{q}{\pi D_1 L}, \text{ Btu/sec-ft}^2 \tag{8}$$

The subcooling in enthalpy units is given by

$$\Delta h_s = h_f - h_1, \text{ Btu/lb} \tag{9}$$

where h_f is the enthalpy of saturated water at pressure P, and h_1 is the enthalpy of water at temperature T_1. (The steam table value for saturated water at temperature T_1 is used.)

The quality at test section exit is given by

$$x_e = \left[\frac{q}{\dot{W}} - \Delta h_s \right] \frac{1}{h_{fg}} \tag{10}$$

The foregoing relationships provide the means for calculation of G, $\bar{\phi}_{bo}$, and x_e directly from the test data.

The second step in reducing the data is to determine, for any given burnout run and for any given position y_i along the rod, the local heat flux ϕ_i and local quality x_i. If y_i is the position of burnout, then ϕ_i and x_i are the heat flux and quality at burnout.

The heat flux as any position y_i is simply

$$\phi_i = \psi_i \ \bar{\phi}_{bo} \tag{11}$$

where $\psi = \psi(y) = \dfrac{dr/dy}{R/L}$, see Figures 2A and 2B. (12)

The quality at the same position is

$$x_i = \frac{1}{h_{fg}} \left[\frac{\bar{\phi}_{bo} \pi D_1 L}{\dot{W}} \left(\frac{r}{R} \right)_i - \Delta h_s \right] \tag{13}$$

where $\dfrac{r}{R} = \dfrac{r}{R}(y)$, see Table 1.

Equations (11) and (13) can be solved together to yield ϕ as a function of x for one particular burnout run.

For purposes of comparison, the uniform rod burnout correlation, Reference 6, is reproduced here.

$$\frac{\phi_{bo(c)}}{10^6} = \frac{\left[1 + 0.16\left(\frac{1000-P}{400}\right) - 0.04\left(\frac{1000-P}{400}\right)^2 \right]}{1 - 0.008\, B\left(\frac{G}{10^6}\right)^{0.8}} \left[0.0172B\left(\frac{G}{10^6}\right)^{0.8} - \left\{ 0.3175\left(\frac{G}{10^6}\right)^{-2} - 1.8534\left(\frac{G}{10^6}\right)^{-1} \right\} - \left\{ 2.4 + 3.2\, D_h + 0.83\, D_h \left(\frac{G}{10^6}\right) \right\} x \left\{ x^2 - 0.0629\left(\frac{G}{10^6}\right)^{-2} + 0.3429\left(\frac{G}{10^6}\right)^{-1} - 0.2494 + 0.0020\left(\frac{G}{10^6}\right)^2 \right\} \right] \tag{14}$$

where $\phi_{bo(c)}$ is in Btu/hr-ft^2; P is in psia; $B = \left(\frac{D_2}{D_1}\right)^{0.5} (D_2 - D_1)^{-0.2}$, D_1 and D_2 are in feet; G is in lb/hr-ft^2; D_h is in inches; and x, the quality, is expressed as a decimal fraction.

The uniform rod correlation is considered valid for the following range of conditions:

Quality:	$-0.12 < x < 0.44$
Flow:	$0.14 < \frac{G}{10^6} < 6.2$ lb/hr-ft^2
Hydraulic Diameter:	$0.25 \leqslant D_h \leqslant 0.875$ inch
Pressure:	$600 \leqslant P \leqslant 1450$ psia
Heat Flux:	$0.35 < \frac{\phi_{bo}}{10^6}$ Btu/hr-ft^2

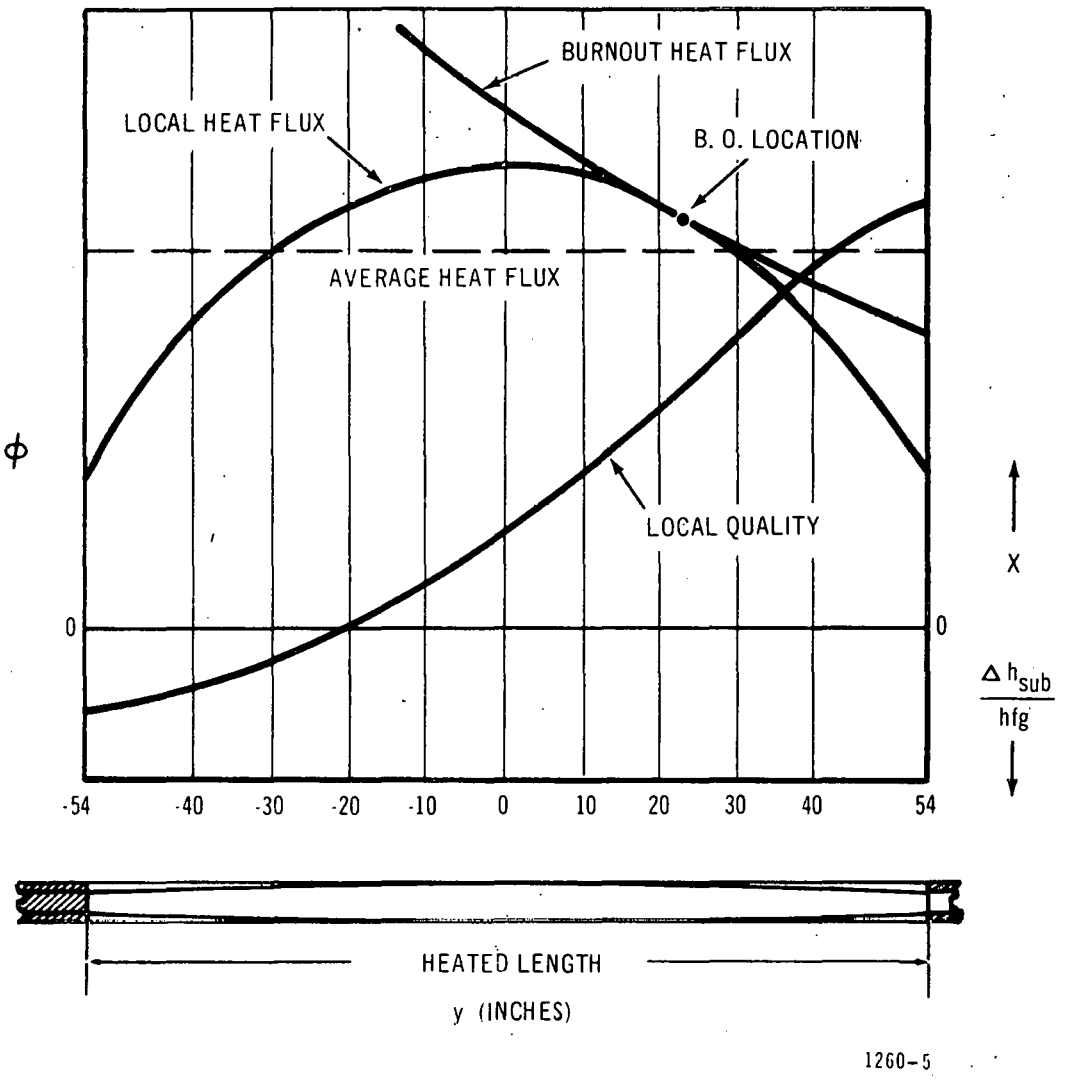

Figure 7. Local Heat Flux, Quality, and Burnout Heat Flux For Typical Rod at Burnout

RESULTS AND DISCUSSION

Burnout runs were made for the flow conditions listed in Table 4. Several runs were made for each flow, the inlet subcooling being adjusted to a different value for each run. The average heat flux at burnout, and the corresponding exit quality for each run, are listed in Table 5, and plotted in Figures 9 and 10 for cosine and truncated cosine, respectively.

The burnout detection circuit indicated burnout and tripped the power for all of the runs except runs numbered 20 and 25. Both of these runs ended in actual burnout. For Run No. 20, the center of the burnout was located at y = 24.4 inches, a position 0.4 inch before one of the spacer pins. A photograph of this burnout is reproduced in Figure 8. For Run No. 25, the center of the burnout was located at approximately y = 53.75 inches, 0.25 inch before the end of the heated section.

The particular thermocouples which were used for voltage taps and for indication of temperature rise are listed, with their locations, in Table 3. The particular thermocouple which indicated a temperature rise at burnout are noted by an asterisk. At least one thermocouple indicated a temperature rise for every run except for runs numbered 25 and 31.

Referring to either Figure 9 or 10, the points for a given flow fall within $\pm$ 10 percent of a straight line, except for two of the points at the lowest flow condition, which are high. The straight line thus defined for the highest flow lies below the corresponding straight lines for the other two flows. In general, for a given exit quality a higher flow results in a lower average heat flux at burnout. This is the same flow effect that has been observed with uniform rod burnout.[6] It will be noted, however, upon comparing Figure 10 with Figure 9, that the flow effect is much less pronounced with the truncated cosine rod than with the cosine.

The local heat flux and quality have been calculated for each run, for the thermocouple positions at which a temperature rise was indicated. These values are listed in Table 6, and are plotted for the three flows, 0.84×10^6, 1.12×10^6, and 1.40×10^6 lb/hr-ft^2, in Figures 11, 12, and 13, respectively. The plots also include the two actual burnout points. Superposed is the uniform rod burnout correlation from Reference 6 for the three flow conditions. Uniform rod burnout points, also from Reference 6, are superposed on Figure 12. In addition to these, the burnout limit curves from Reference 8 are superposed. These limit curves represent the lower bounds for all the data points of Reference 6. It will be seen that they also bound the low side of the data points of Figures 11, 12, and 13.

Referring to Figure 11, at the 0.84×10^6 lb/hr-ft^2 condition, the cosine rod points are quite consistent with the truncated cosine points. All of the data could be fitted by a single straight line, with a scatter of less than $\pm$ 15 percent. The average is about 20 percent below the uniform rod correlation.

TABLE 5

COSINE ROD BURNOUT

D_1 = 0.540-Inch
D_2 = 0.875-Inch
D_h = 0.335-Inch
L = 108 Inches

Run No.	Rod No.	P psia	$\frac{G}{10^6}$ lb/hr-ft^2	Δh_{oub} Btu/lb	$\frac{\bar{\phi}_{bo}*}{10^6}$ Btu/hr-ft^2	x_e*	Remarks
C-1	4	1000	1.11	36.6	0.504	0.288	
C-2	59	1005	1.12	172.2	0.740	0.236	
C-3	59	1005	1.12	21.3	0.471	0.288	
C-4	59	1005	0.84	24.7	0.414	0.337	
C-5	59	1005	0.84	57.1	0.448	0.316	
C-6	59	1005	0.84	94.2	0.504	0.311	
C-7	59	1003	0.84	149.3	0.600	0.312	
C-8	59	1001	0.84	199.9	0.665	0.291	
C-9	59	1004	0.84	252.3	0.748	0.288	
C-10	59	1000	0.84	300.2	0.836	0.296	
C-11	59	1005	0.83	130.9	0.560	0.309	
C-12	59	1002	0.84	106.8	0.536	0.323	
C-13	59	1002	0.84	151.5	0.590	0.301	
C-14	59	1003	0.84	50.3	0.456	0.334	
C-15	59	1000	0.84	25.6	0.430	0.351	
C-16	59	1005	1.40	17.2	0.484	0.236	
C-17	59	1000	1.40	62.3	0.575	0.216	
C-18	59	1000	1.40	116.1	0.680	0.190	
C-19	59	1000	1.39	162.0	0.783	0.177	
C-20	59	1005	1.39	297.6	1.120	0.152	Actual burnout at y = 24.4
C-21	42	1000	1.40	64.2	0.600	0.225	
C-22	42	1000	1.37	120.8	0.708	0.207	
C-23	42	1000	1.40	11.8	0.504	0.255	
C-24	42	1000	1.11	252.0	0.886	0.219	
C-25	42	1000	1.12	306.5	0.990	0.200	Actual burnout at y = 53.75

*Note that the last two columns are the average heat flux and the exit quality at burnout. The heat flux and quality at burnout position may be different.

TABLE 5 (Continued)

TRUNCATED COSINE ROD BURNOUT

D_1 = 0.540-Inch D_h = 0.335-Inch

D_2 = 0.875-Inch L = 91 Inches

Run No.	Rod No.	P psia	$\frac{G}{10^6}$ lb/hr-ft^2	Δh_{sub} Btu/lb	$\frac{\bar{\phi}_{bo}*}{10^6}$ Btu/hr-ft^2	x_e*	Remarks
C-26	20	1015	1.39	28	0.572	0.223	
C-27	20	991	1.39	67	0.669	0.205	
C-28	20	1003	1.40	113.5	0.759	0.173	
C-29	20	1003	1.40	113.5	0.745	0.166	
C-30	20	1000	1.40	218	0.994	0.119	
C-31	7	1000	1.14	37.5	0.548	0.251	
C-32	7	1000	1.14	67	0.601	0.235	
C-33	7	1005	1.14	98	0.659	0.218	
C-34	7	1005	1.14	118	0.696	0.210	
C-35	7	1000	1.13	200	0.850	0.173	
C-36	7	1005	1.13	241.5	0.964	0.176	
C-37	18	1005	0.85	39	0.464	0.289	
C-38	18	1005	0.84	75	0.497	0.263	
C-39	18	1005	0.84	77.5	0.499	0.260	
C-40	18	1005	0.84	108	0.548	0.249	
C-41	18	1005	0.85	139	0.589	0.230	
C-42	18	1000	0.85	144	0.592	0.226	
C-43	18	1000	0.85	193	0.675	0.213	
C-44	18	1005	0.83	219	0.726	0.222	
C-45	18	1005	0.83	268.5	0.805	0.210	
C-46	18	1010	0.85	268	0.818	0.200	
C-47	18	995	1.12	217	0.864	0.159	
C-48	18	1000	1.13	234	0.900	0.149	

*Note that the last two columns are the average heat flux and the exit quality at burnout. The heat flux and quality at the burnout position are different.

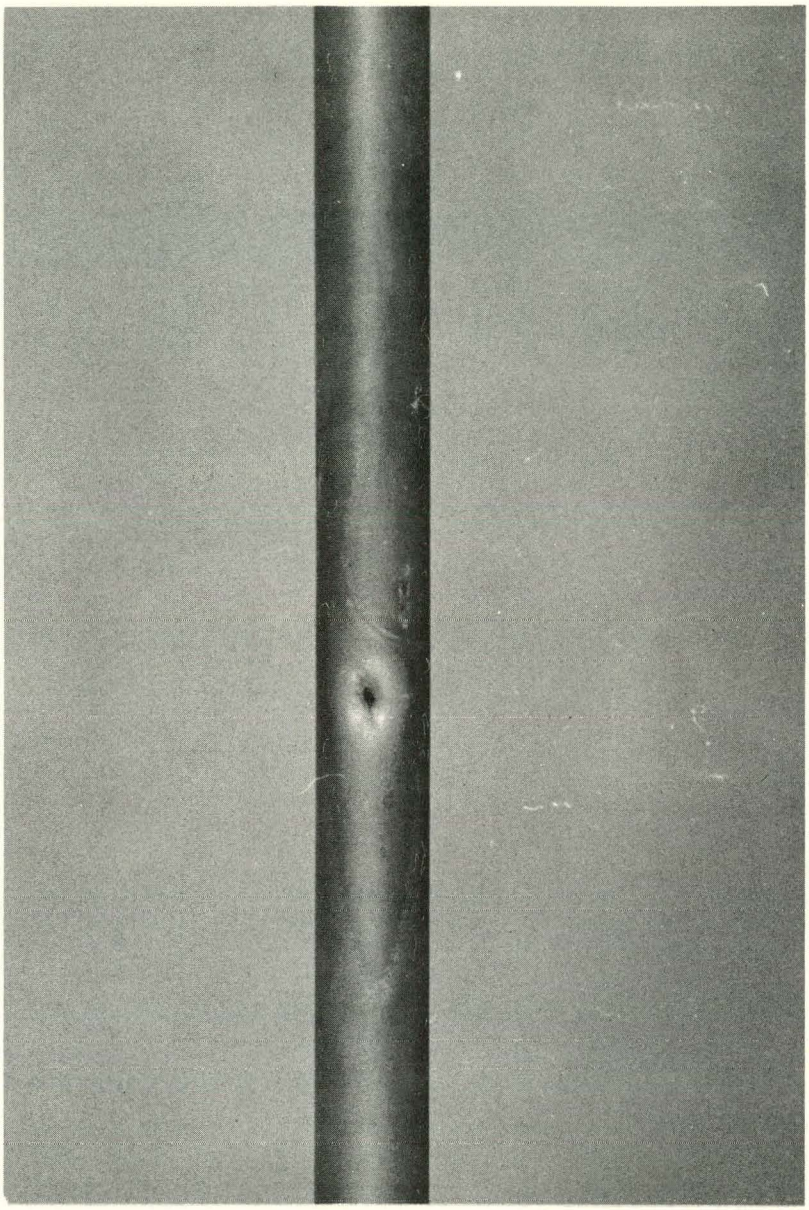

1760-26

Figure 8. Actual Burnout, Run No. 20 - Cosine Rod

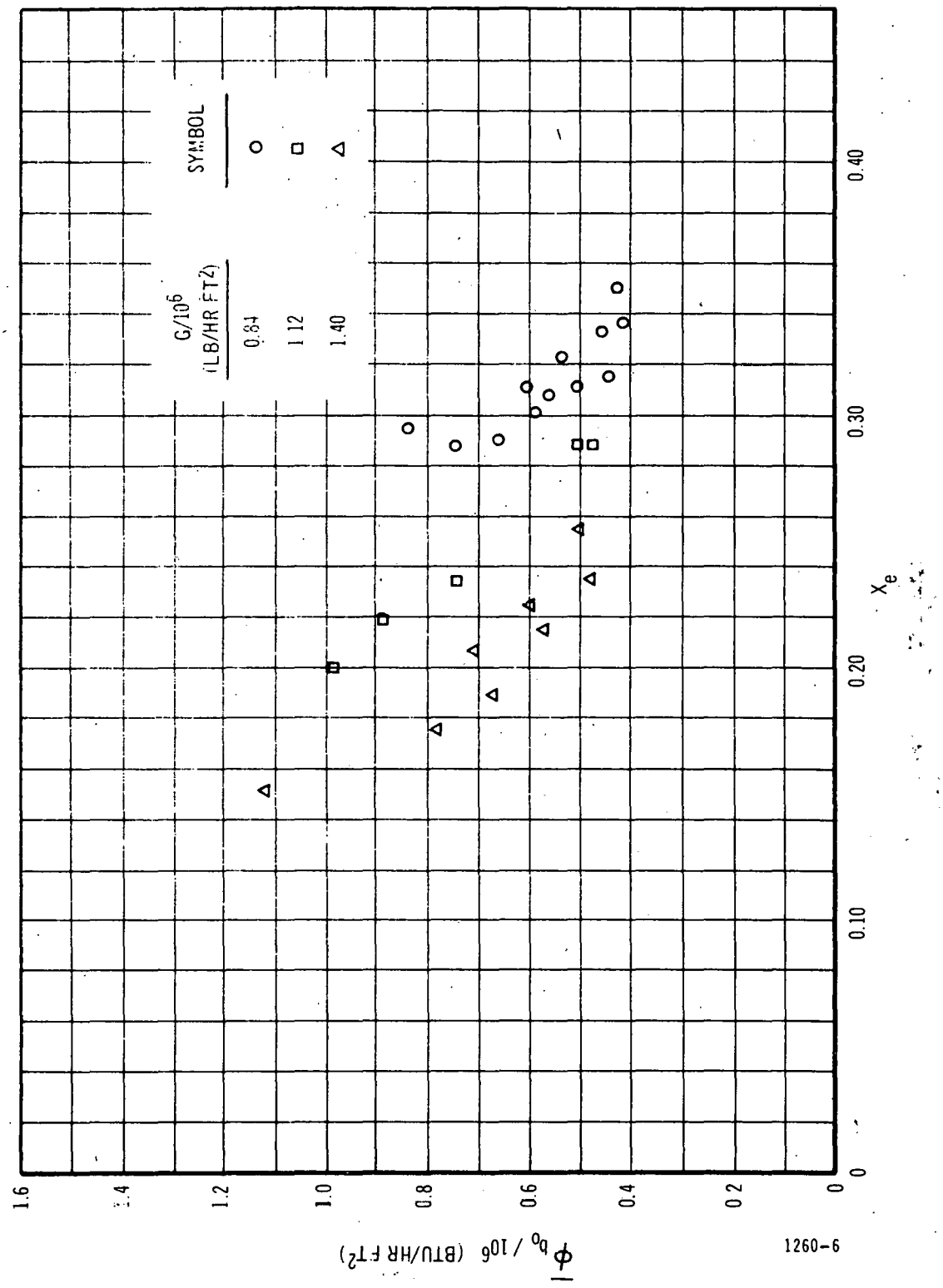

Figure 9. Average Heat Flux at Burnout vs. Exit Quality - Cosine Rod

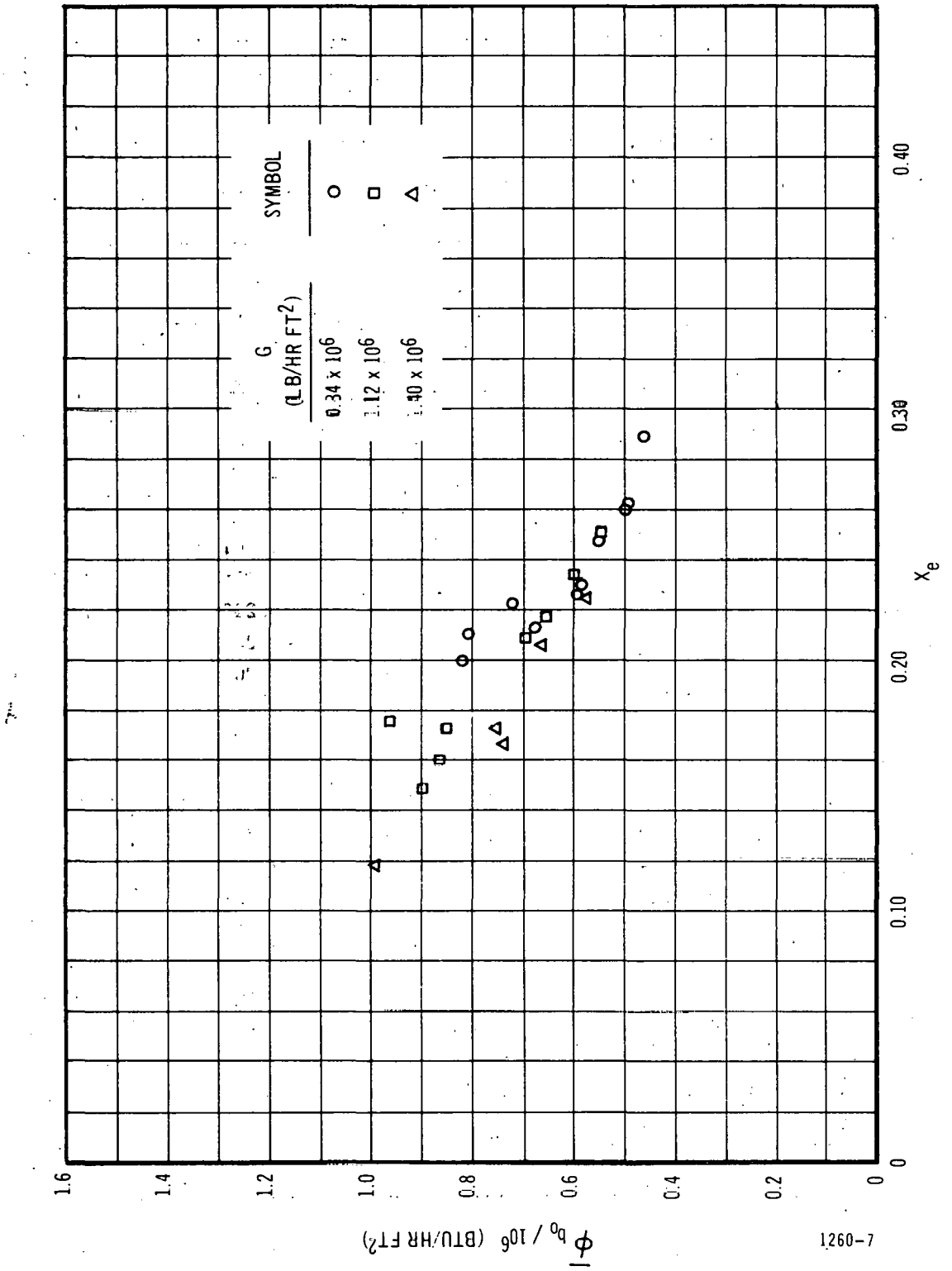

Figure 10. Average Heat Flux at Burnout vs. Exit Quality - Truncated Cosine Rod

TABLE 6

HEAT FLUX AND QUALITY AT POSITION OF TEMPERATURE RISE INDICATION

Run No.	$\frac{G}{10^6}$	Temperature Rise at y=	x_i	$\frac{\phi_i}{10^2}$
1	1.11	44	0.266	0.369
2	1.12	34	0.167	0.688
3	1.12	34	0.245	0.438
		43	0.266	0.337
4	0.84	34	0.287	0.385
		43	0.311	0.296
5	0.84	34	0.261	0.416
		43	0.295	0.321
6	0.84	34	0.249	0.468
7	0.84	34	0.239	0.557
8	0.84	34	0.209	0.618
9	0.84	34	0.200	0.695
10	0.84	34	0.192	0.778
11	0.83	34	0.240	0.521
12	0.84	34	0.256	0.498
13	0.84	34	0.227	0.549
14	0.84	34	0.279	0.424
15	0.84	34	0.298	0.400
16	1.40	34	0.201	0.450
17	1.40	34	0.173	0.535
18	1.40	34	0.140	0.633
19	1.39	34	0.119	0.728
		37	0.130	0.664
20	1.39	25	0.014	1.309
21	1.40	49	0.199	0.410
22	1.37	49	0.196	0.404
23	1.40	25	0.194	0.580
		49	0.245	0.350
24	1.11	49	0.200	0.606
25	1.12	-		
26	1.39	31	0.207	0.552
27	1.39	31	0.191	0.645
28	1.40	31	0.153	0.733

TABLE 6 (Continued)

Run No.	$\frac{G}{10^6}$	Temperature Rise at y =	x_i	$\frac{\phi_i}{10^2}$
29	1.40	31	0.148	0.728
30	1.40	29	0.082	1.005
31	1.14	-		
32	1.14	27	0.202	0.637
		29	0.209	0.604
		31	0.217	0.570
		33	0.223	0.532
		33.6	0.331	0.456
33	1.14	31	0.198	0.625
34	1.14	31	0.187	0.660
35	1.13	19	0.076	0.988
		27	0.124	0.900
		29	0.136	0.855
		31	0.145	0.804
		33	0.154	0.752
36	1.13	31	0.142	0.913
37	0.85	29	0.260	0.482
		31	0.267	0.453
		33	0.274	0.425
38	0.84	31	0.240	0.487
		33	0.248	0.456
39	0.84	31	0.238	0.489
		33	0.246	0.458
40	0.84	31	0.225	0.536
		33	0.234	0.503
41	0.85	31	0.202	0.577
		33	0.211	0.540
42	0.85	31	0.195	0.580
		33	0.205	0.543
43	0.85	33	0.189	0.619
		36.6	0.208	0.537
44	0.83	31	0.189	0.712
		33	0.200	0.665
		36.6	0.220	0.577
45	0.83	33	0.182	0.739
46	0.85	31	0.165	0.802
		33	0.177	0.750
47	1.12	31	0.131	0.846
48	1.13	29	0.108	0.936
		31	0.120	0.882

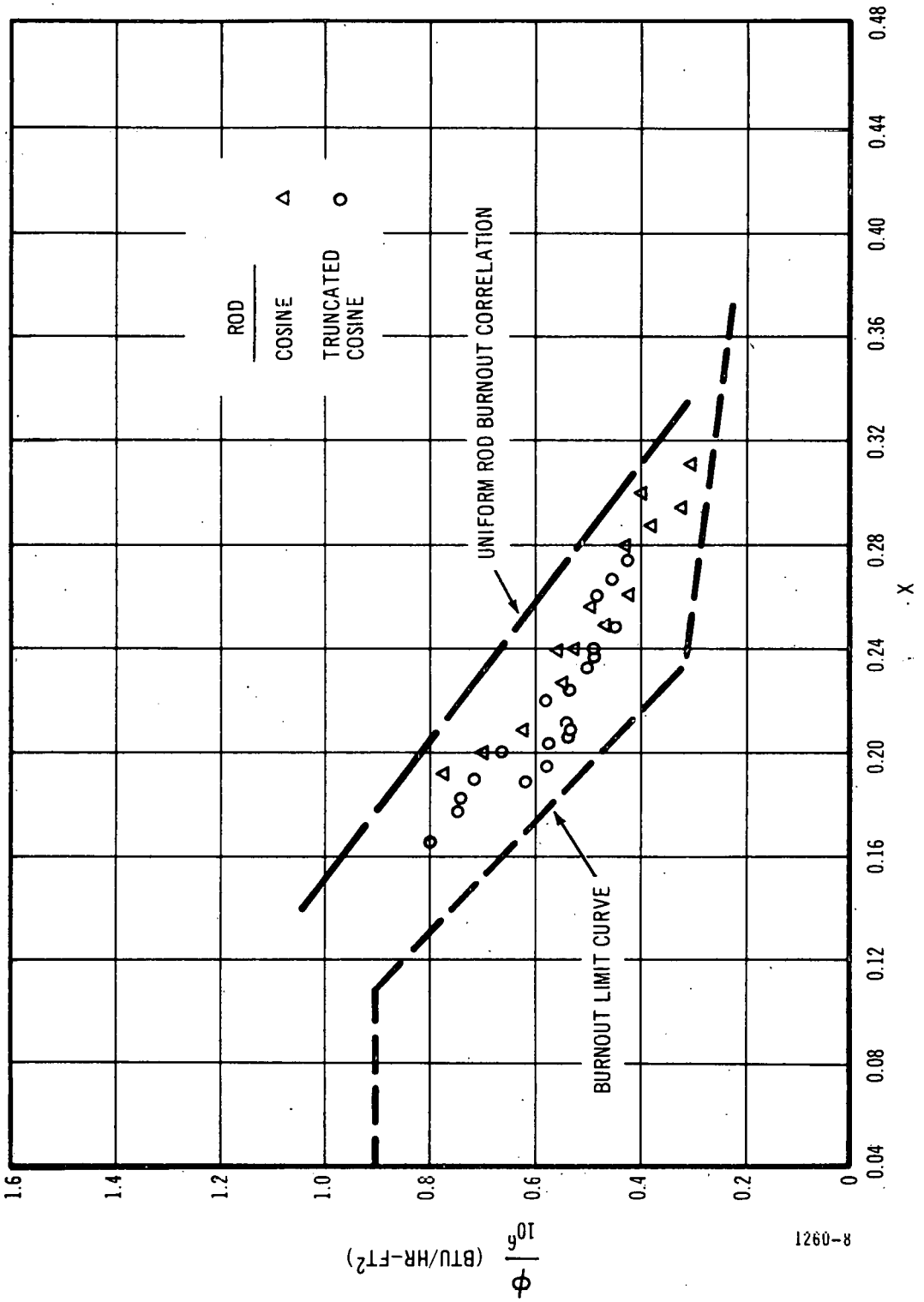

Figure 11. Heat Flux vs. Quality at Position of Temperature Rise Indication
$G = 0.84 \times 10^6$ lb/hr-ft^2

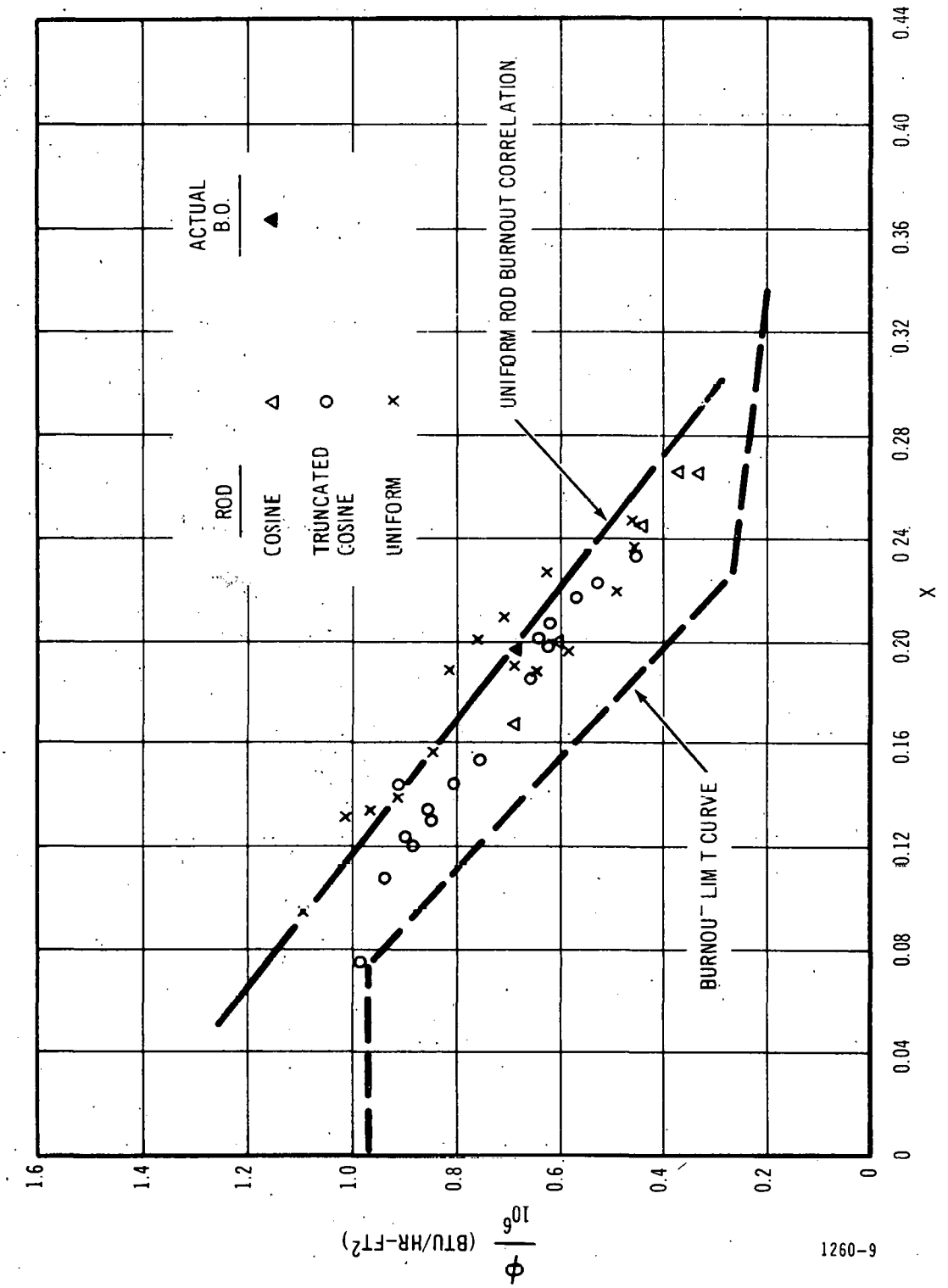

Figure 12. Heat Flux vs. Quality at Position of Temperature Rise Indication
$G = 1.12 \times 10^6$ lb/hr-ft^2

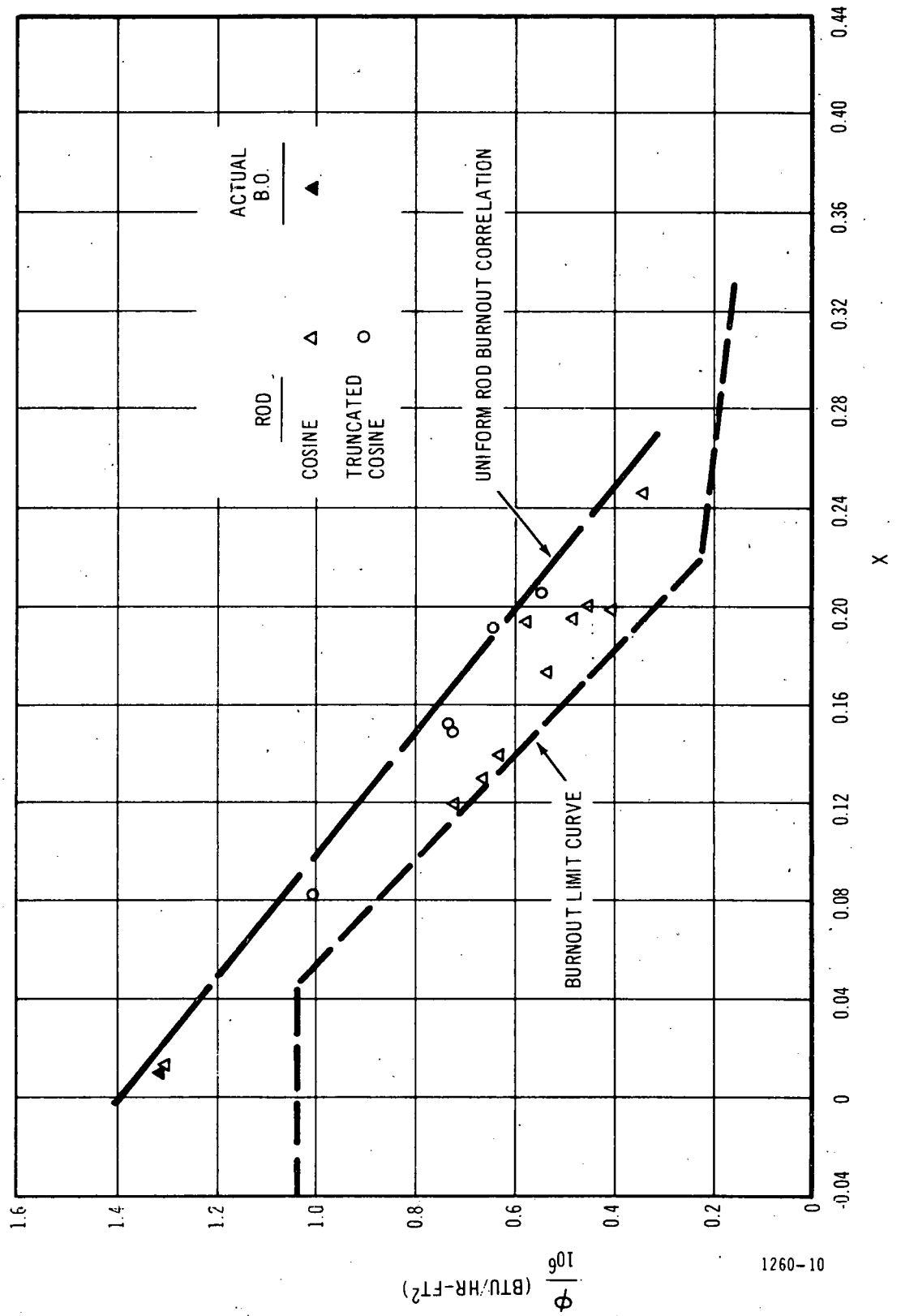

Figure 13. Heat Flux vs. Quality at Position of Temperature Rise Indication
$G = 1.40 \times 10^6$ lb/hr-ft^2

Putting it another way, 50 percent of the points fall within -7 percent, -20 percent of the uniform rod correlation, and 94 percent fall within -7 percent, -30 percent of the uniform rod correlation. Note the burnout limit curve of Reference 8, which lies below all the points.

Referring to Figure 12, at the 1.12×10^6 lb/hr-ft^2 condition, the cosine rod points are also quite consistent with the truncated cosine points, although the former tend to be a little low. All of the cosine and truncated cosine data could be fitted by a single straight line, with a scatter of less than $\pm$ 12 percent. The average is about 9 percent below the uniform rod correlation. Sixty-eight percent of the points fall within +1 percent, -10 percent of the correlation, and all of the points fall within +1 percent, -20 percent of the correlation.

It may be noted that the cosine and truncated cosine data are in good agreement with the uniform data. It is also interesting to note that the actual burnout point lies exactly on the correlation. The burnout limit curve of Reference 8 lies below all the points.

Referring to Figure 13, at the 1.40×10^6 lb/hr-ft^2 condition, the cosine rod points tend to be low with respect to the truncated cosine points. Even so, all of the data could be fitted by a single straight line with a scatter of $\pm$15 percent or less. The average is about 10 percent below the uniform rod correlation. Fifty percent of the points fall within +3 percent, -10 percent of the correlation. 69 percent fall within +3 percent, -20 percent of the correlation, and all of the points fall within +3 percent, -30 percent of the correlation. It may be noted again that the actual burnout point lies very close to (within 3 percent) the correlation. As before, the burnout limit curve of Reference 8 lies below all the points.

In summary of Figures 11 through 13, the cosine and truncated cosine data are from 9 percent to 20 percent low, with respect to the uniform rod correlation. The medium and high flow data are in better agreement with the correlation than are the low flow data. Except for the low flow condition, the cosine points tend to be low with respect to the truncated cosine. Considering all of the cosine and truncated cosine points, 70 percent fall within +3 percent, -20 percent, and 96 percent fall within +2 percent, -30 percent of the uniform rod correlation. * As has already been pointed out, all of the points lie above the burnout limit curves of Reference 8.

Further insight can be gained by plotting a continuous curve of local heat flux versus local quality for certain representative runs. This has been done for the cosine rod at the flow 0.84×10^6, 1.12×10^6, and 1.40×10^6 lb/hr-ft^2, in Figures 14, 15, and 16, and for the truncated cosine rod at the same flows in Figures 17, 18, and 19. Each of the curves represents the conditions along the rod which existed for one burnout run, from y = 6 inches to the exit end of the rod. The position of each thermocouple which indicated a temperature rise, the position of any actual burnout, and the position of the three voltage taps used for burnout detection, are all marked on each curve. Superposed on each plot is the uniform rod burnout correlation.

*The correlation itself was based on 362 uniform rod data points, 95 percent of which fall within $\pm$20 percent, and 99 percent within $\pm$30 percent (Reference 5).

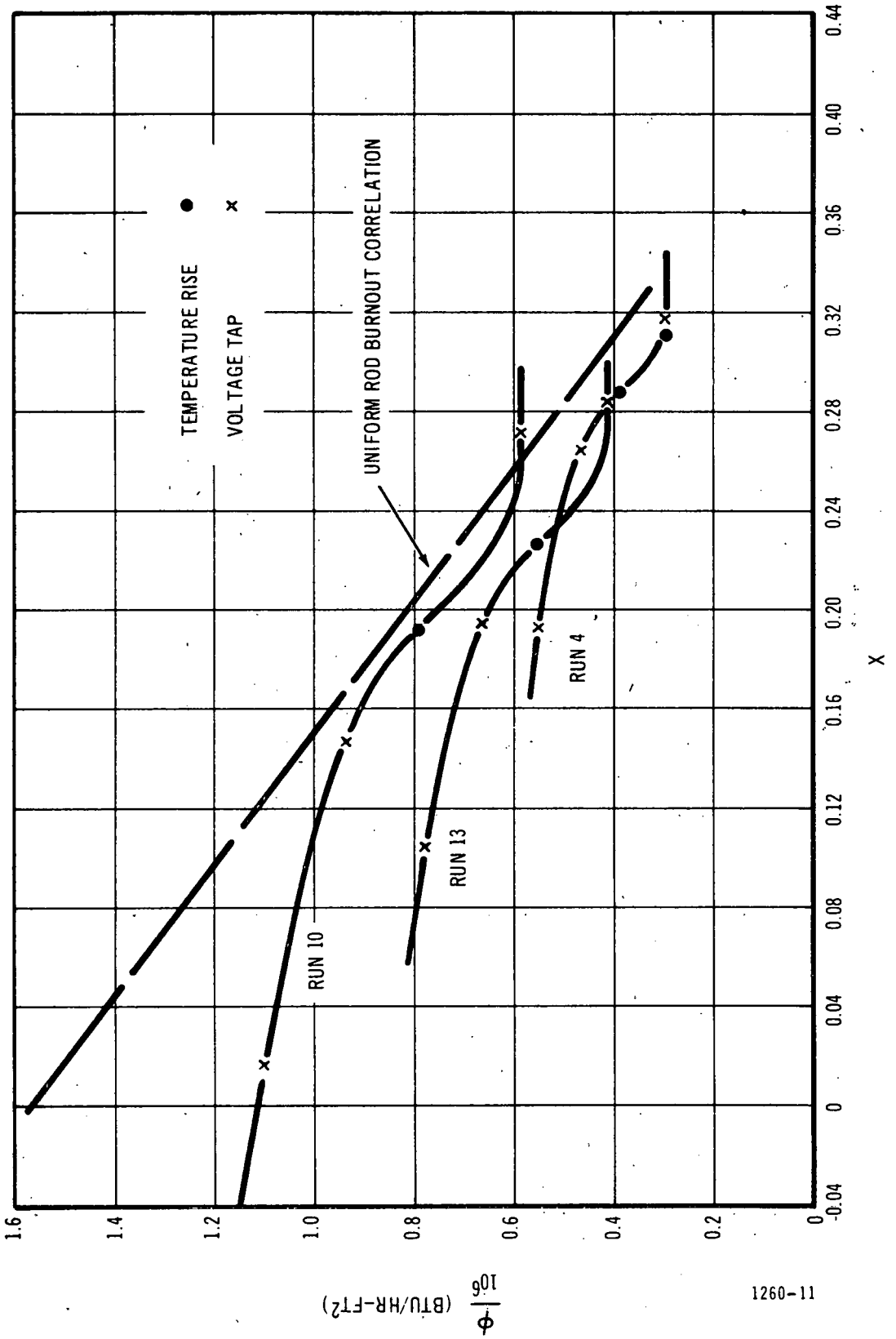

Figure 14. Local Heat Flux vs. Local Quality at Burnout - Cosine Rod
$G = 0.84 \times 10^6$ lb/hr-ft^2

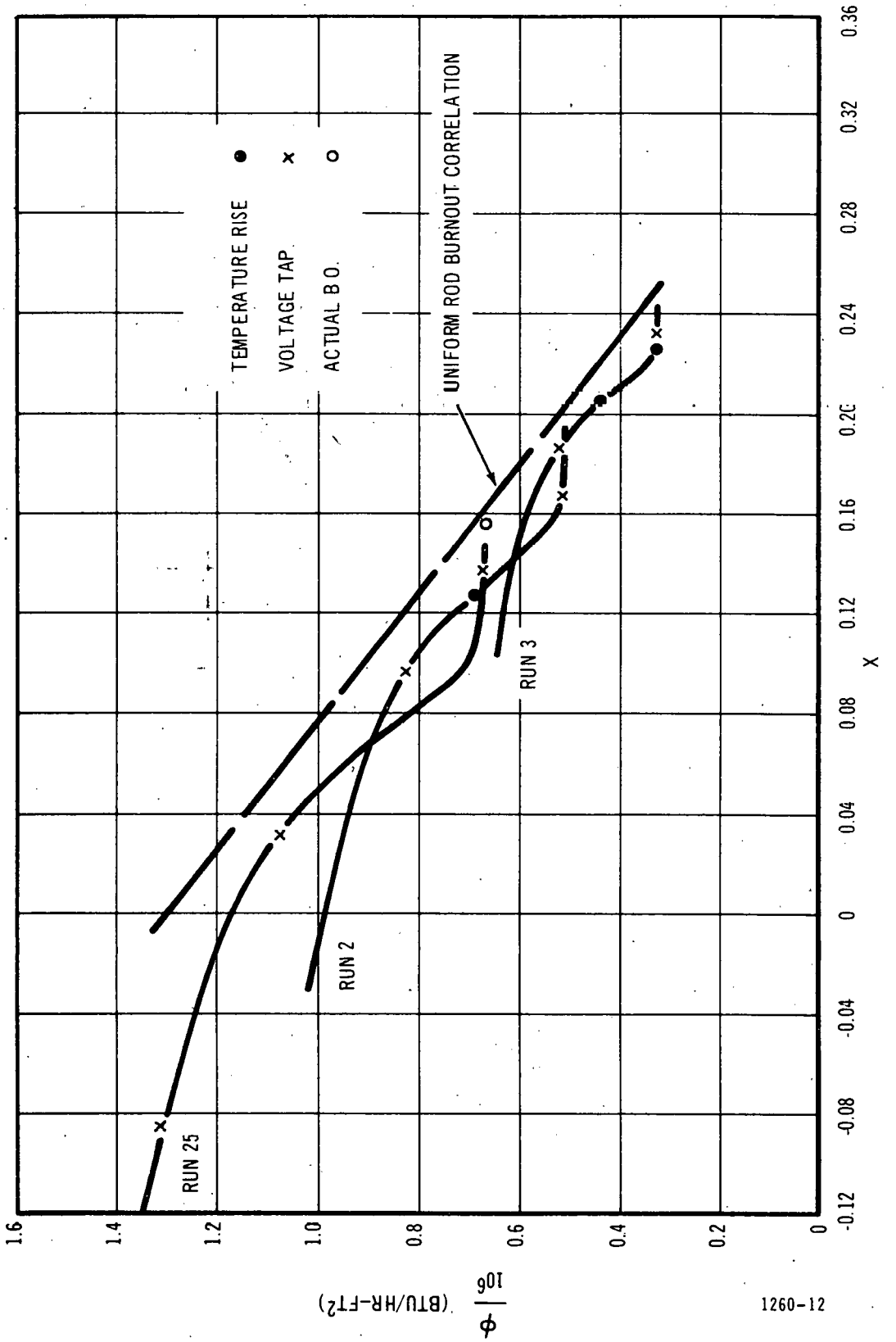

Figure 15. Local Heat Flux vs. Local Quality - Cosine Rod
$G = 1.12 \times 10^6$ lb/hr-ft^2

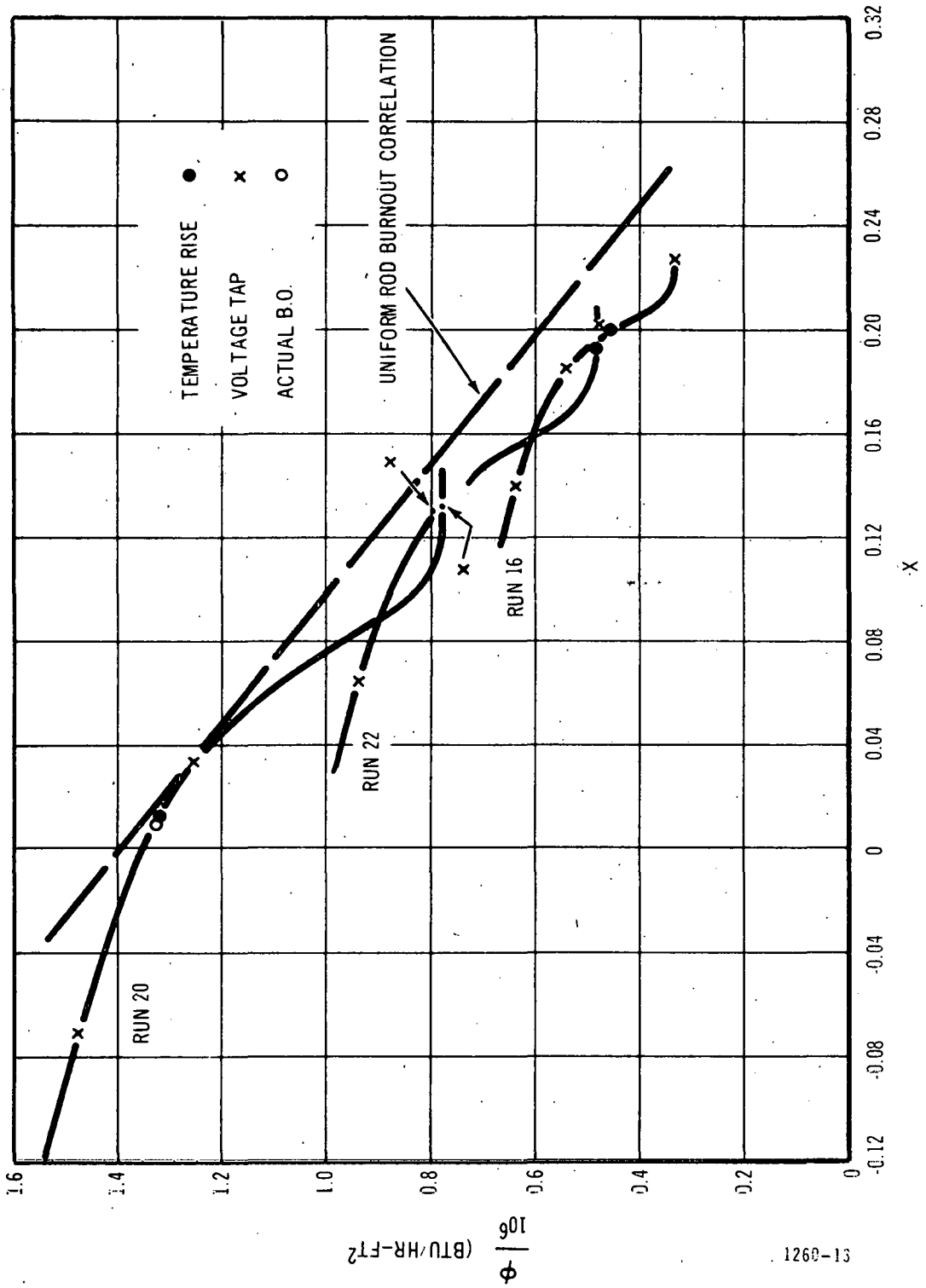

Figure 16. Local Heat Flux vs. Local Quality - Cosine Rod
$G = 1.40 \times 10^6$ lb/hr-ft^2

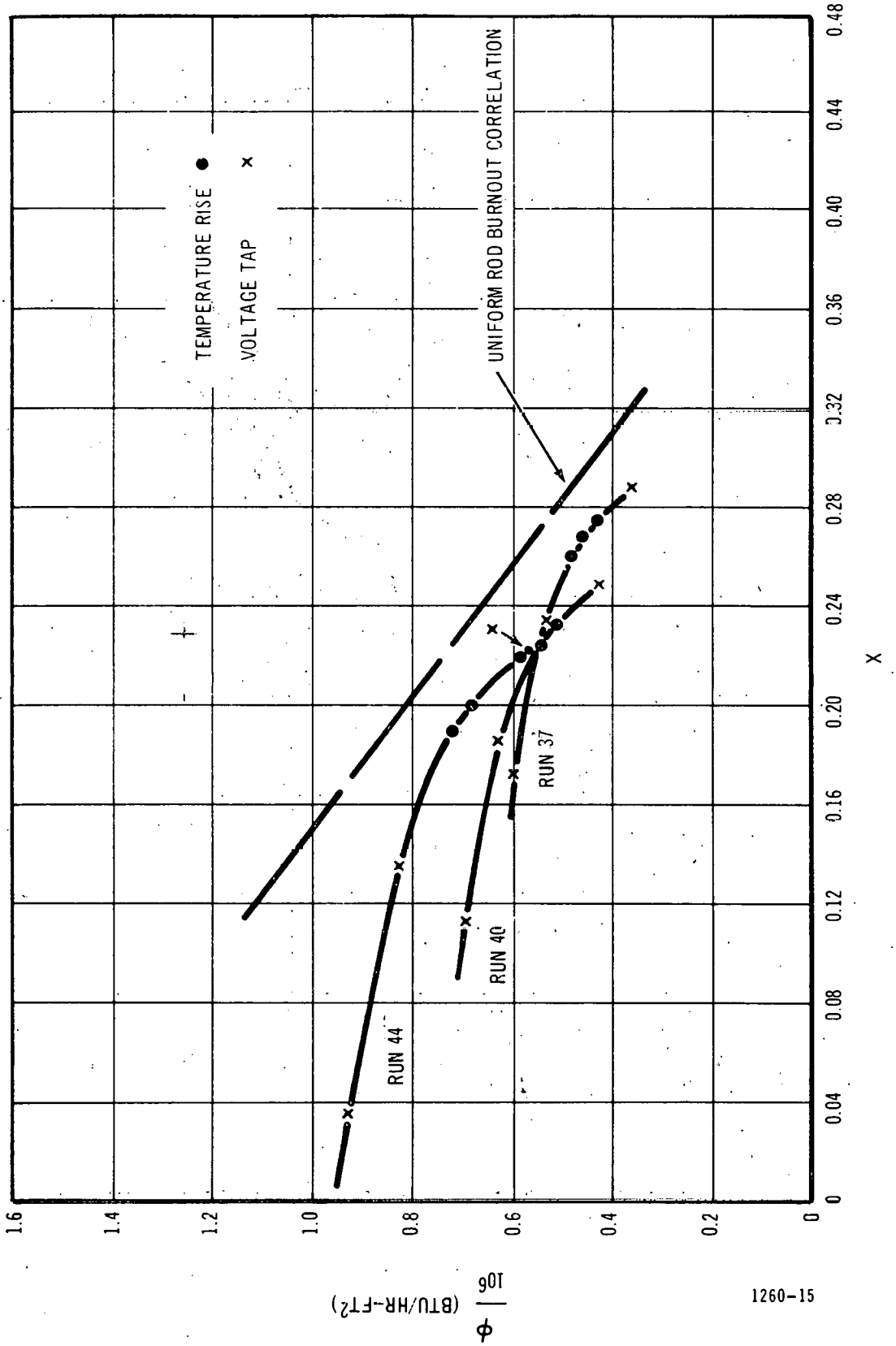

Figure 17. Local Heat Flux vs. Local Quality - Truncated Cosine Rod
$G = 0.84 \times 10^6$ lb/hr-ft^2

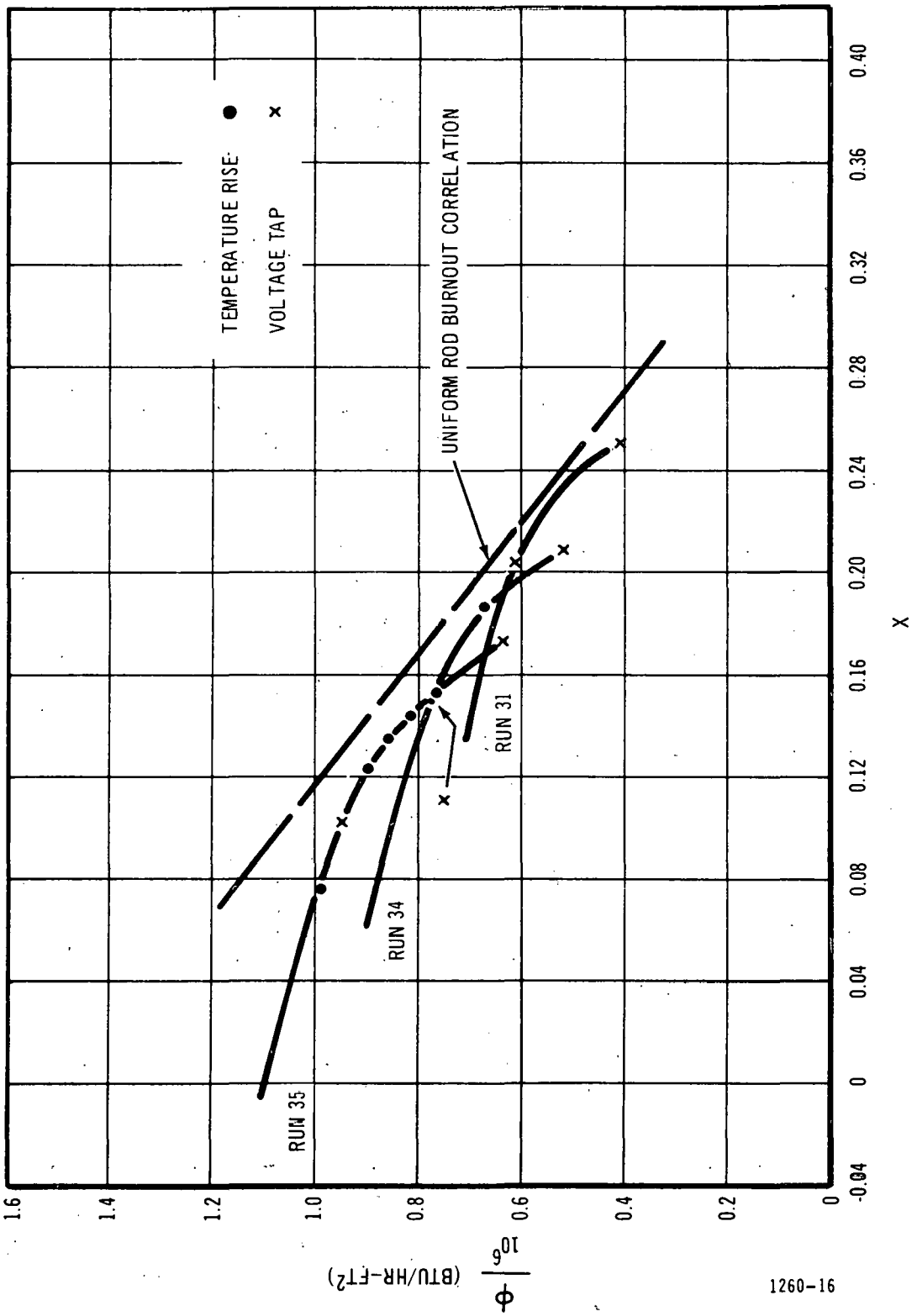

Figure 18. Local Heat Flux vs. Local Quality - Truncated Cosine Rod
$G = 1.12 \times 10^6$ lb/hr-ft^2

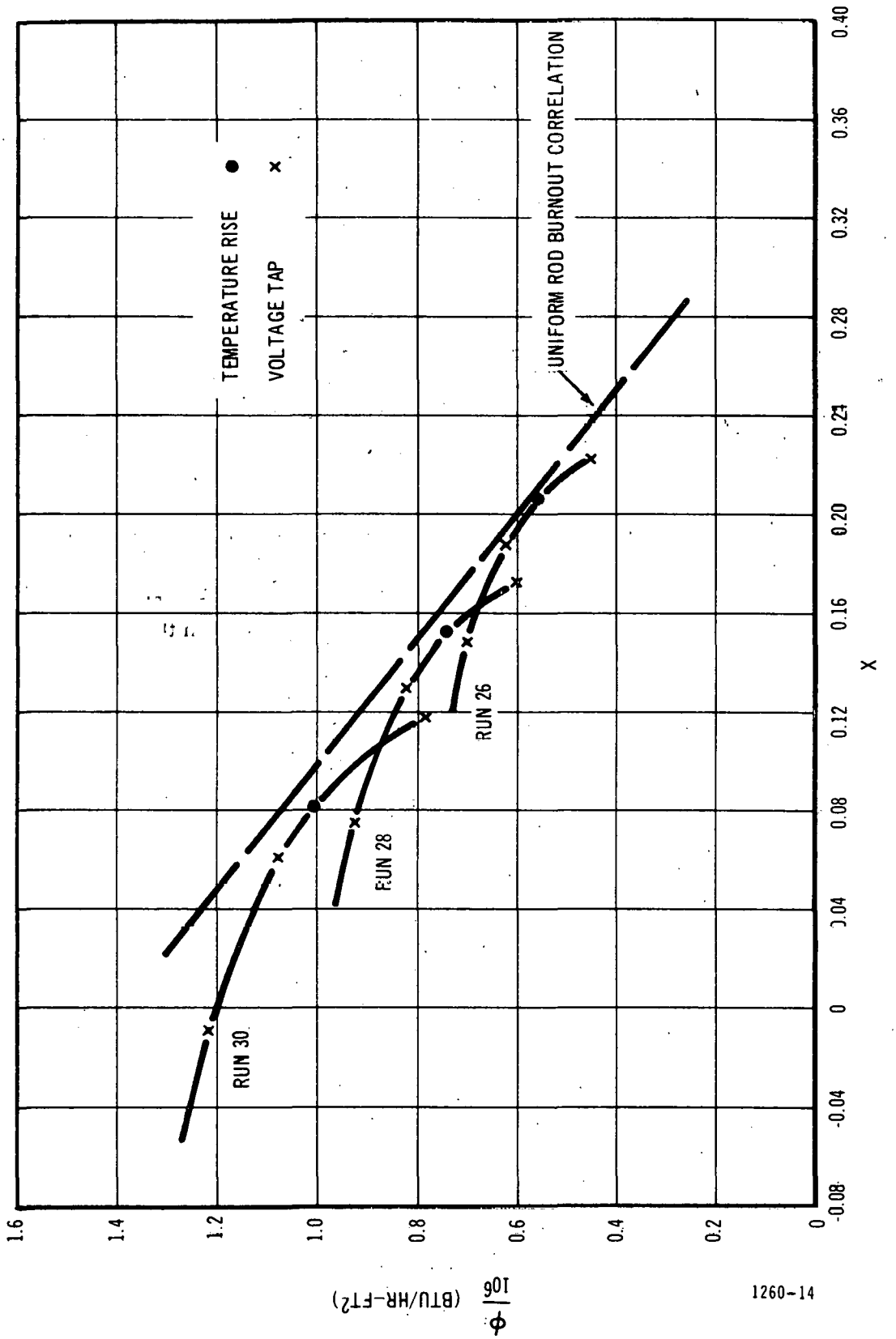

Figure 19. Local Heat Flux vs. Local Quality - Truncated Cosine Rod
$G = 1.40 \times 10^6$ lb/hr-ft^2

The first voltage tap is the tap nearest the exit end of the rod. The burnout detector functions to indicate a burnout if there is a temperature rise anywhere between the first and second taps. It may be noted that at least one thermocouple did indicate a temperature rise in this region for every run except numbers 25 and 31. The region experiencing temperature rise was probably more extensive than indicated by the thermocouple(s).

Some parts of the rod containing no thermocouples (particularly the cosine rod, Figures 14, 15, and 16) were much closer to (in some cases above) the uniform rod correlation than the parts with thermocouples which indicated temperature rise. It is believed that a burnout condition existed in some of the noninstrumented parts, which would generally be in very good agreement with the uniform rod correlation. The actual burnout point of Run No. 25 is evidence that this is so.

It has already been noted that the cosine and truncated cosine data show a small (9 percent to 20 percent) reduction in burnout heat flux relative to the uniform rod correlation. However, the percent deviation of the cosine and truncated cosine data from the uniform rod correlation is small and the same order as that for the uniform rod data upon which the correlation was originally based. It is concluded from this, plus the other evidence of agreement with the correlation, that the correlation can be used in predicting burnout for cosine power distribution. *

It is tacit in the above conclusion that burnout depends only on local conditions. Burnout is independent of axial gradients in heat flux, for gradients at least as steep as those of the cosine and truncated cosine rods. It is conceivable that a gradient could be so extreme that this would no longer hold (see, for example, the "hot patch" tests of Reference 2), but the gradients encountered in reactor practice should have no effect on burnout.

Burnout is independent of the heated length ahead of it, a fact already observed for uniform rods for heated lengths from 108 inches down to 29 inches (Reference 6), unless the heated length is extremely short (so short, for example, that the flow at the test section inlet is already two-phase). The heated lengths encountered in reactor practice should have no effect on burnout.

It is obvious from the foregoing that no correlation of nonuniform with uniform burnout data would be expected simply on the basis of total power to the test section or inlet enthalpy. ** The correlation with uniform rod results must be on the basis of local conditions.

---

* A procedure for doing this is described in the next section.

** The statement made in Reference 9, based on an incorrect interpretation of preliminary findings reported in Reference 10, that "... Cook found ... for a given inlet enthalpy and flow rate, DNB occurred at the same power input for both a uniform and cosine power distribution", is in error. Reference 11 also contains an incorrect interpretation of Reference 10, which leads to the erroneous conclusion that, "Because the cosine data points coincide with the straight line obtained from a uniform flux, we can conclude that DNB depends only on power input (or ΔH_{DNB}) to the channel and is independent of the local peak heat flux." The conclusion reported in Reference 10, that "It is evident from these curves that burnout with nonuniform power distribution may be reliably predicted from uniform power distribution data", is in agreement with the findings in this report.

PREDICTION OF BURNOUT FOR A NONUNIFORMLY HEATED ROD

The analysis upon which this prediction of burnout is based is given in the Appendix. It is postulated in the analysis that burnout is independent of gradients in the heat flux, and depends only on local quality and flow. Therefore, the local heat flux at burnout is the same as for a uniform rod, which, according to the uniform rod correlation, can be expressed by

$$\phi_{bo} = A - B\,x \tag{15}$$

It is shown in the analysis that at the burnout position

$$\frac{d \ln \psi}{dy} = - \frac{B \pi D_1}{\dot{W} h_{fg}} \tag{16}$$

The location of burnout y, may be determined by plotting $\frac{d \ln \psi}{dy}$ versus y and superposing a horizontal straight line whose ordinate is $- \frac{B \pi D_1}{\dot{W} h_{fg}}$. Such plots have been prepared for the test rods in Figures 20 and 21. The straight line intersects the curve at the predicted position of burnout. Note that for a given pressure and flow, the position of burnout is invarient, regardless of subcooling Δh_s, and power level $\bar{\phi}_{bo}$.

The predicted heat flux at burnout is given by

$$\phi_{bo(p)} = \frac{\left[A + B \frac{\Delta h_s}{h_{fg}}\right]}{1 + \frac{B \pi D_1 L}{\dot{W} h_{fg}} \frac{(r/R)_1}{\psi_1}} \tag{17}$$

where the constants are the same as in equation (15), and $(\frac{r}{R})_1$ and ψ_1 are functions of y_1. Thus the heat flux at burnout depends on the position of burnout y_1, on the constants for the uniform rod burnout curve, equation (15), and on the inlet subcooling Δh_s. For a given geometry, pressure, and flow, ϕ_{bo} varies linearly with the subcooling.

If it should happen that $\frac{d \ln \psi}{dy} > - \frac{B \pi D_1}{\dot{W} h_{fg}}$ at $y = y_e$, then the location of burnout may be at $y = y_e$, i. e., at the exit end of the rod. If this is so, the heat flux at burnout can be determined from equation (17) by letting $r/R = 1$ and $\psi_1 = \psi_e$.

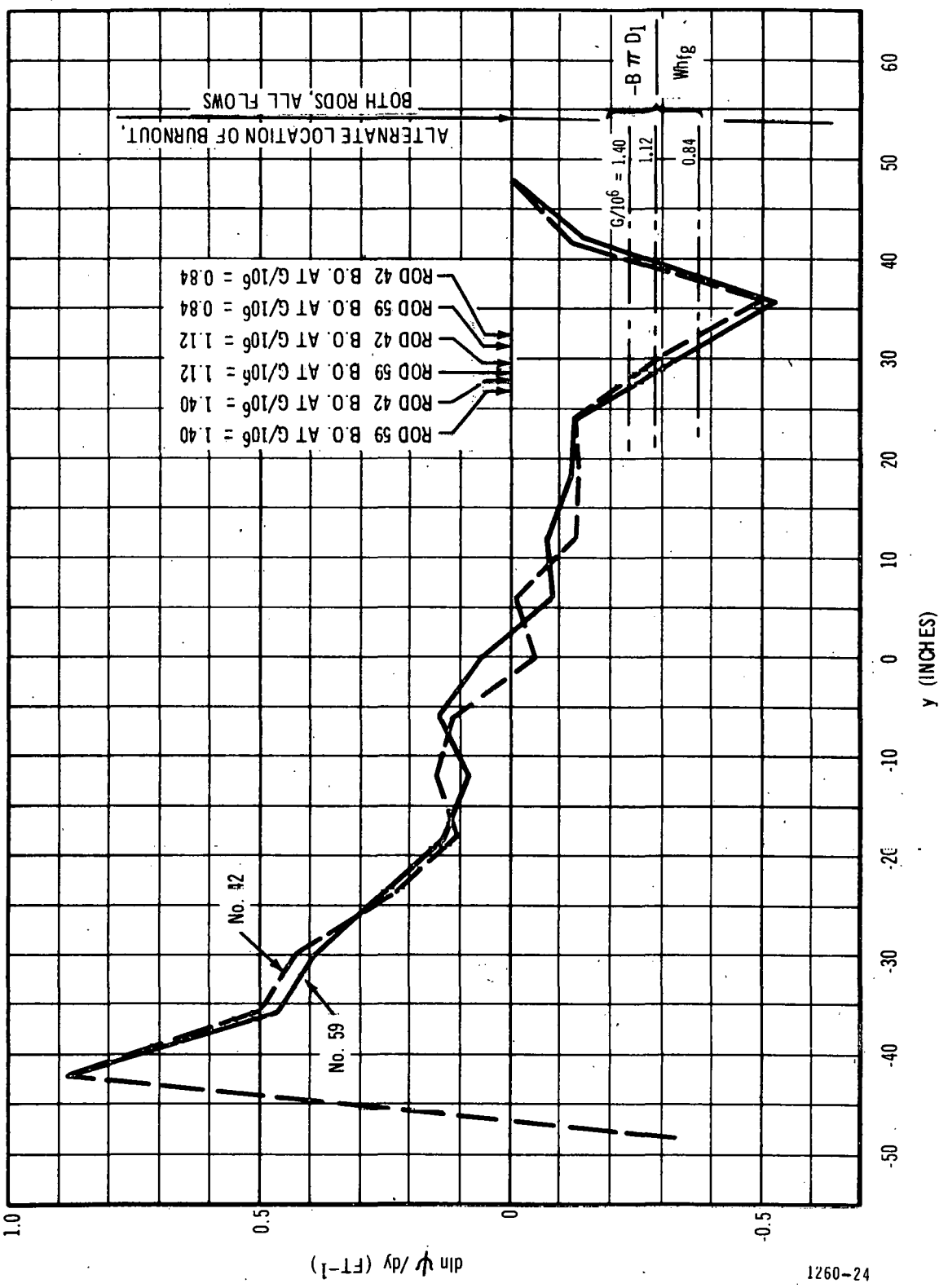

Figure 20. Cosine Rod

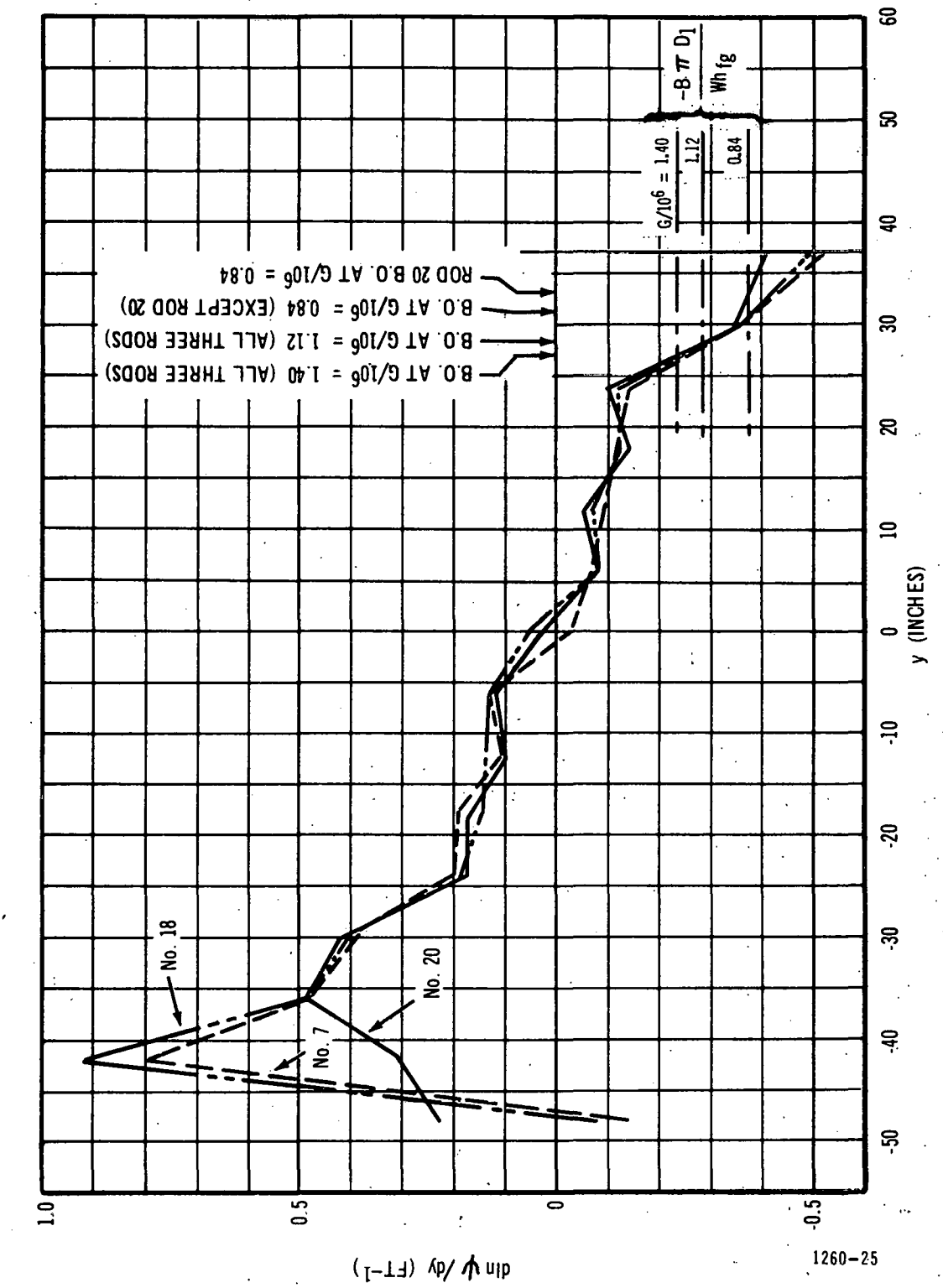

Figure 21. Truncated Cosine Rod

$$\phi_{bo(p)} = \frac{A + B\dfrac{\Delta h_s}{h_{fg}}}{1 + \dfrac{B\pi D_1 L}{\dot{W} h_{fg}} \dfrac{1}{\psi_e}} \tag{18}$$

The predicted average heat flux at burnout is given simply by

$$\bar{\phi}_{bo} = \frac{\phi_{bo}}{\psi_1} \tag{19}$$

Based on the foregoing, the predicted average heat flux at burnout has been calculated for all of the cosine and truncated cosine runs, and is plotted versus the measured average heat flux in Figure 22. All of the points fall within +11 percent, - 2-1/2 percent of a 45 degree line through the origin. This is considered excellent agreement. It must be pointed out, however, that the prediction of average heat flux at burnout requires first that the position of burnout be predicted, and this predicted position did not necessarily agree with the thermocouple data indicating temperature rise. Let us consider this matter further.

The local heat flux and local quality are plotted versus y for certain representative runs, in Figures 23 through 28. The position of each thermocouple which indicated a temperature rise, also the position of any actual burnout, and finally the position of predicted burnout, are all marked on each plot. A curve of the burnout heat flux based on the uniform rod correlation is superposed.

Refer first to the plots for the cosine rod, Figures 23, 24, and 25. It will be noted that the position of predicted burnout positions does not, in most cases, coincide with the positions of indicated temperature rise. The local heat flux at the predicted burnout position is, in every case, the highest value relative to the burnout heat flux curve; it may even extend above the burnout heat flux curve (e. g., Run No. 10). The local heat flux at the position(s) of indicated temperature rise is always lower, relative to the burnout heat flux curve. It must be pointed out, however, that no thermocouple was located closer than 3 inches from the predicted position of burnout except for Run No. 20, and in the case of Run No. 20, the thermocouple did indicate a temperature rise. Moreover, the two actual burnouts occurred at, or very close to, the predicted burnout position (Runs numbered 20 and 25). Even though the direct evidence is incomplete, it is probable that a burnout condition existed at the predicted burnout position for every cosine rod run.

Refer to the plots for the truncated cosine rod, Figures 26, 27, and 28. Here, the position of predicted burnout coincides, or is very close to, the position of indicated temperature rise in every

case (except Run No. 31, for which there was no indicated temperature rise). The local heat flux at the predicted burnout position is again the highest value relative to the burnout heat flux curve. A burnout condition existed at the predicted burnout position for every truncated cosine run.

It is concluded that the method of burnout prediction described here, accomplishes the following, for the degree of nonuniformity of power distribution encountered in reactor practice:

1. Predicts the most probable position at which burnout will occur.
2. Accurately predicts the power level at which burnout will occur.

If burnout conditions exist at other than the predicted position, the heat flux at the other positions will still agree with the heat flux given by the single rod burnout correlation, to within the same order of error as the uniform data upon which the correlation was based.

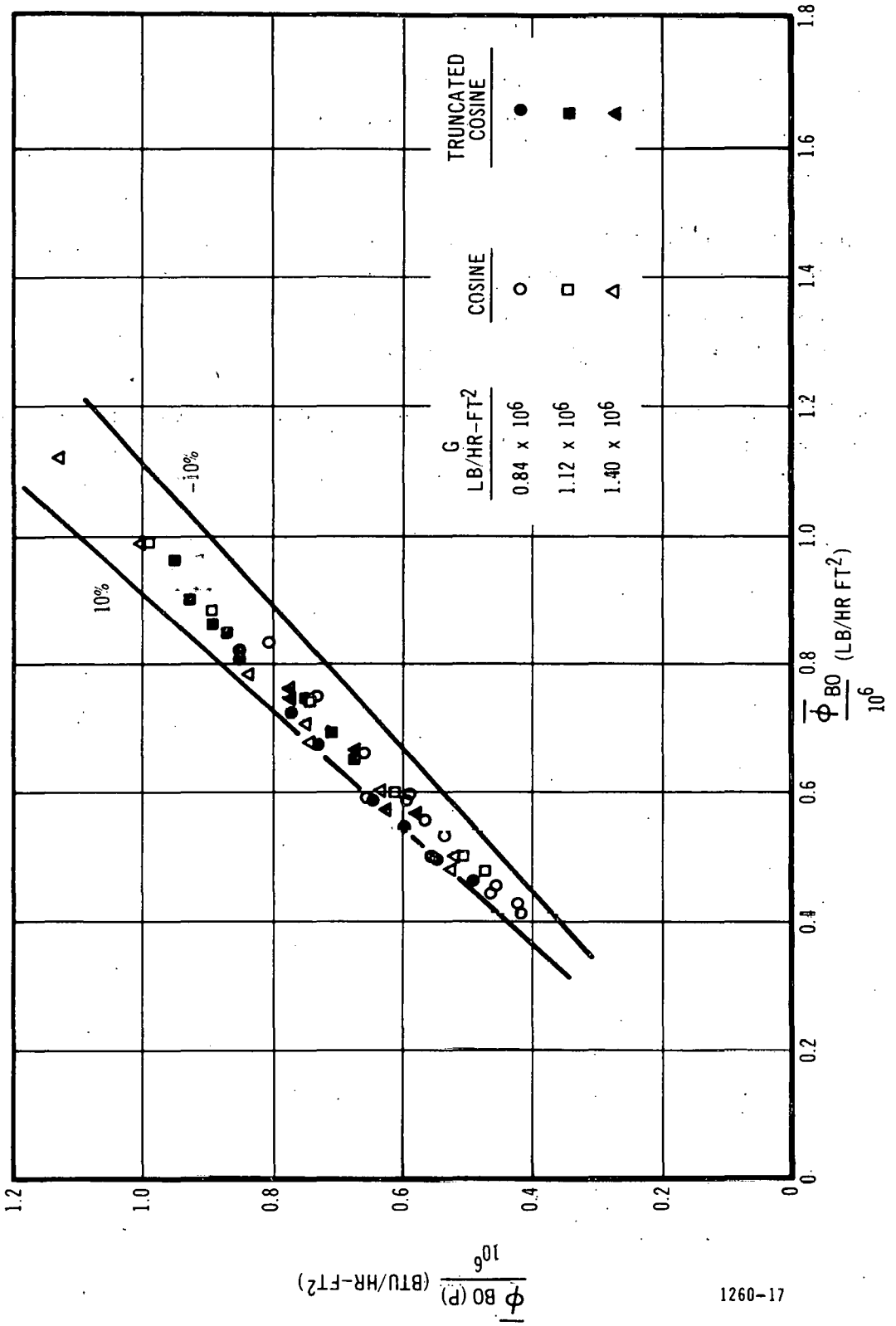

Figure 22. Predicted Average Heat Flux vs. Measured Average Heat Flux

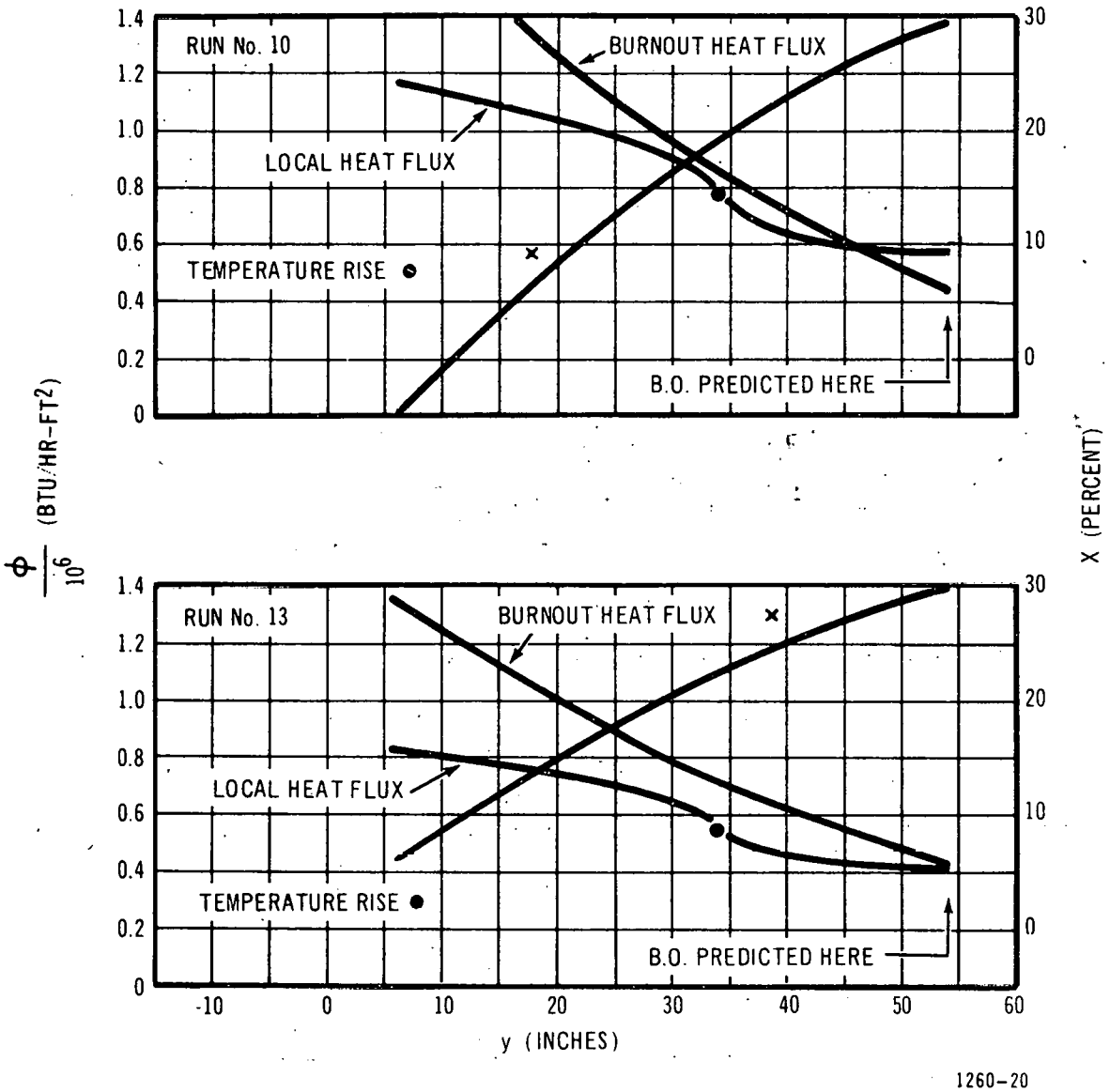

Figure 23. Cosine Rod
$G = 0.84 \times 10^6$ lb/hr-ft^2

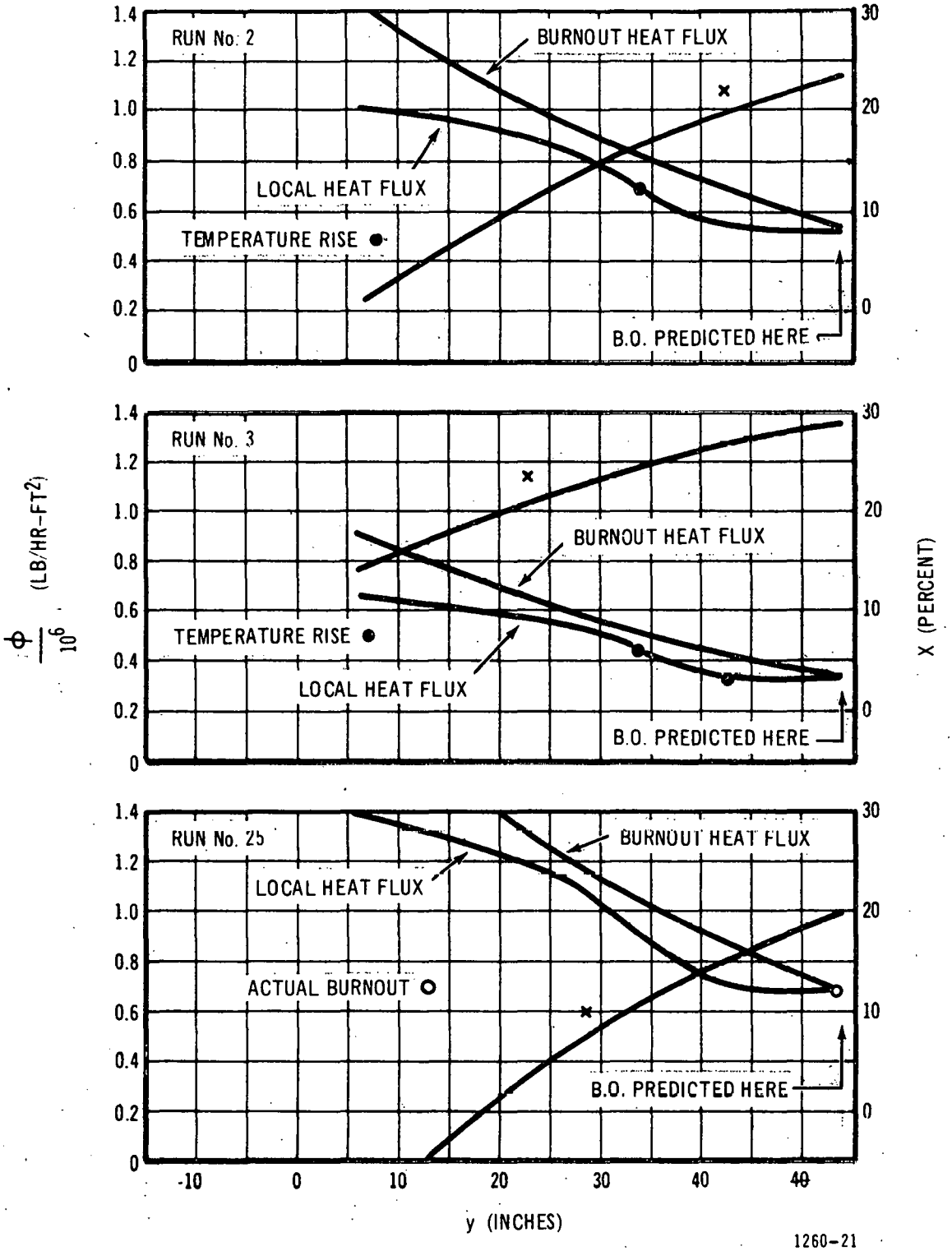

Figure 24. Cosine Rod
$G = 1.12 \times 10^6$ lb/hr-ft^2

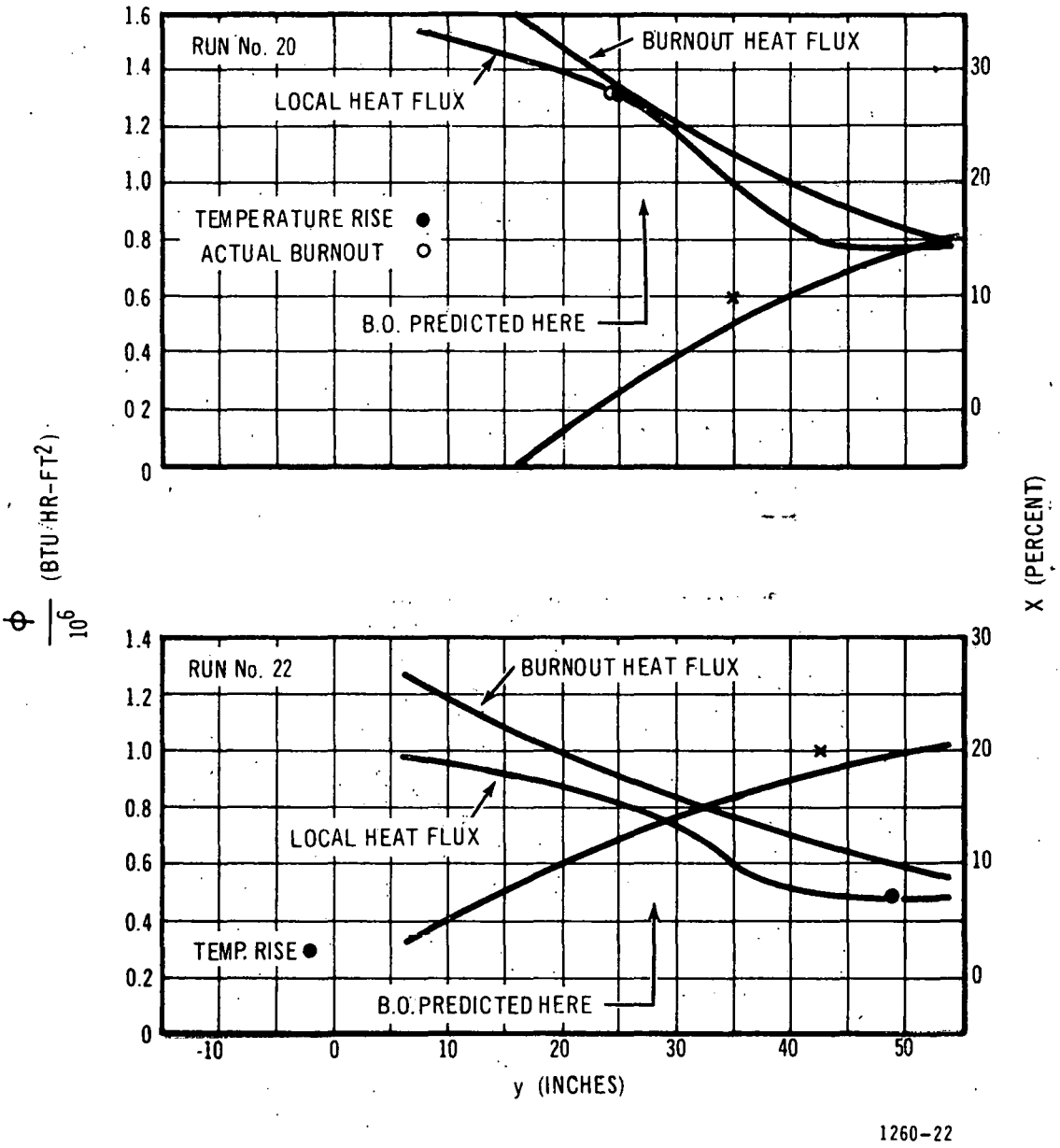

Figure 25. Cosine Rod
$G = 1.40 \times 10^6$ lb/hr-ft^2

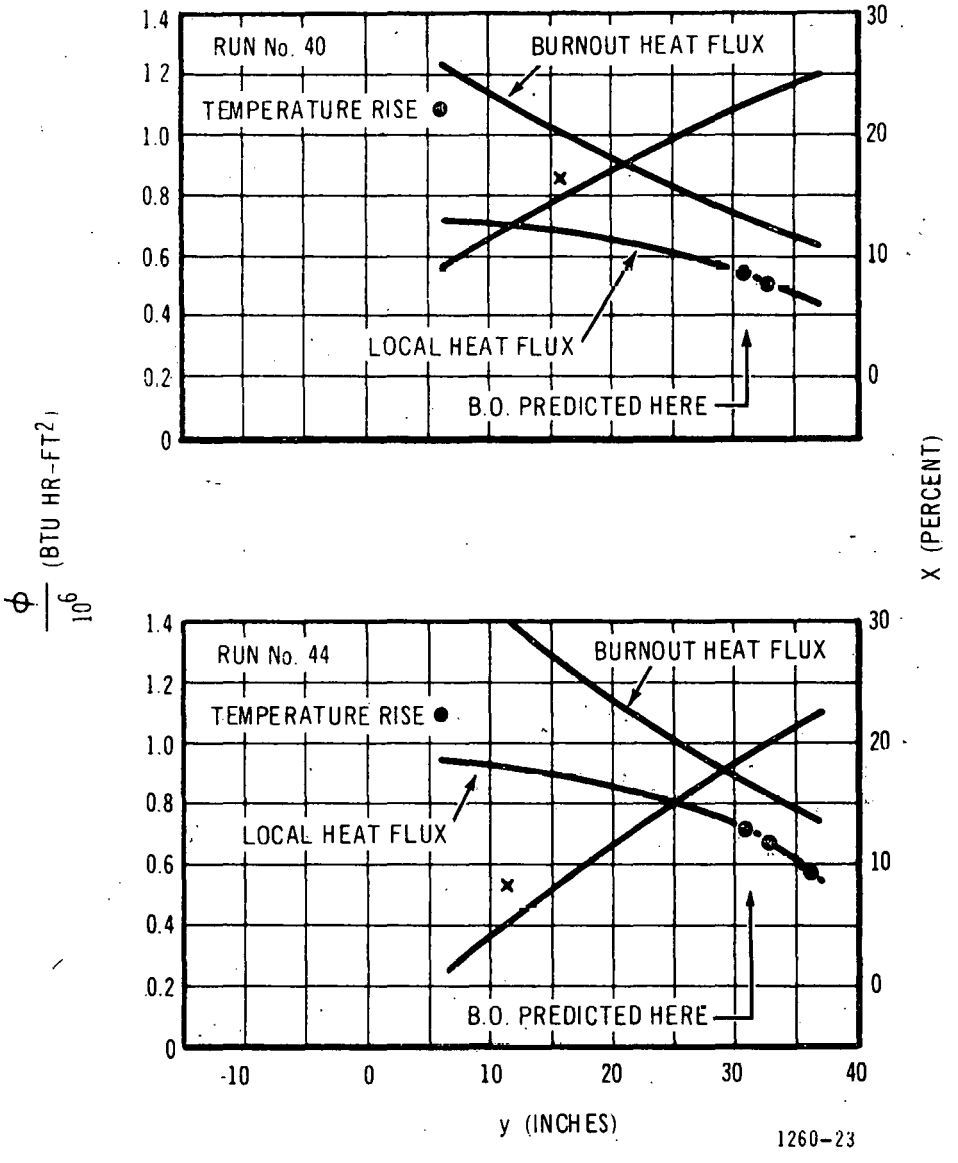

Figure 26. Truncated Cosine Rod
$G = 0.84 \times 10^6$ lb/hr-ft^2

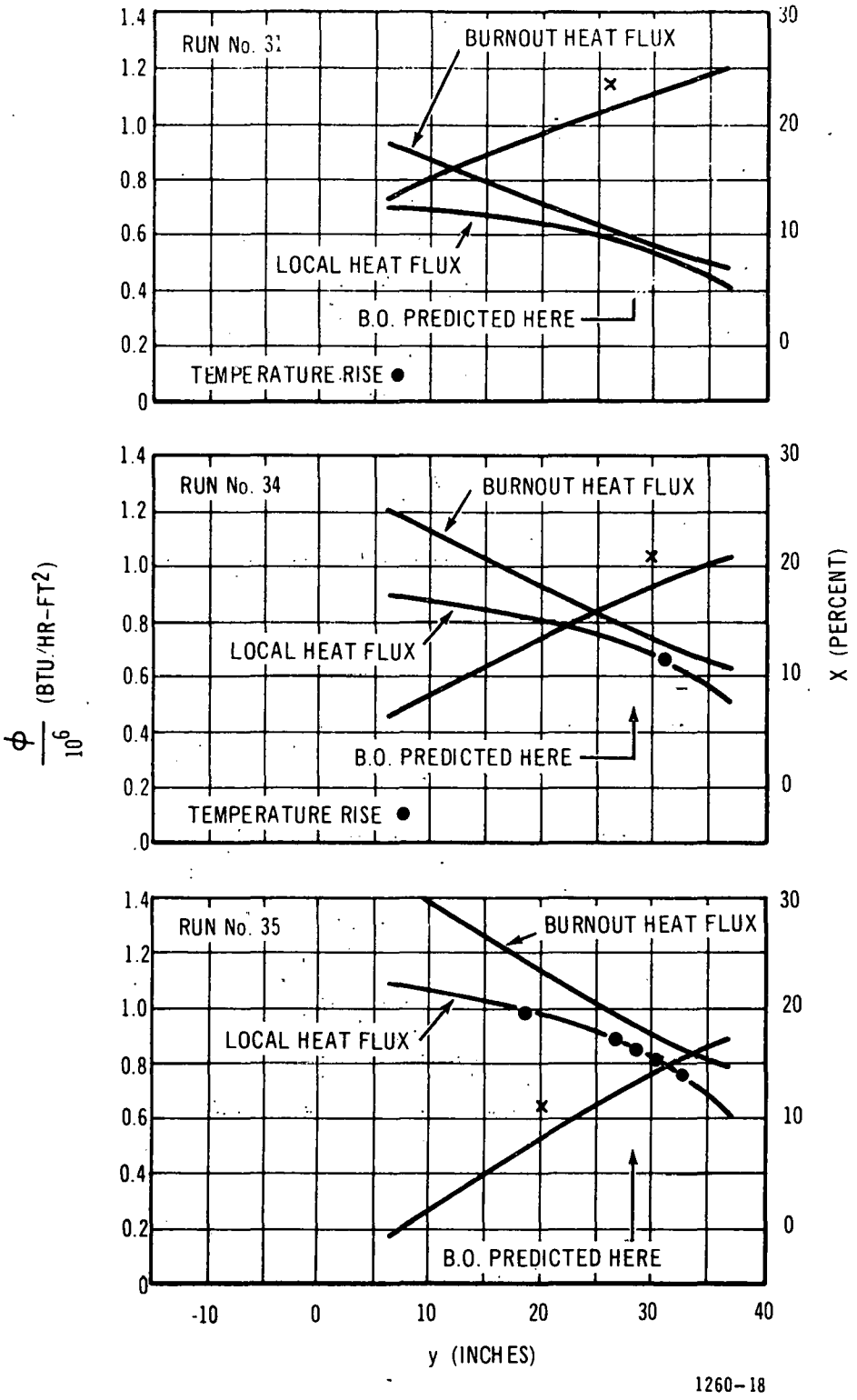

Figure 27. Truncated Cosine Rod
$G = 1.12 \times 10^6$ lb/hr-ft^2

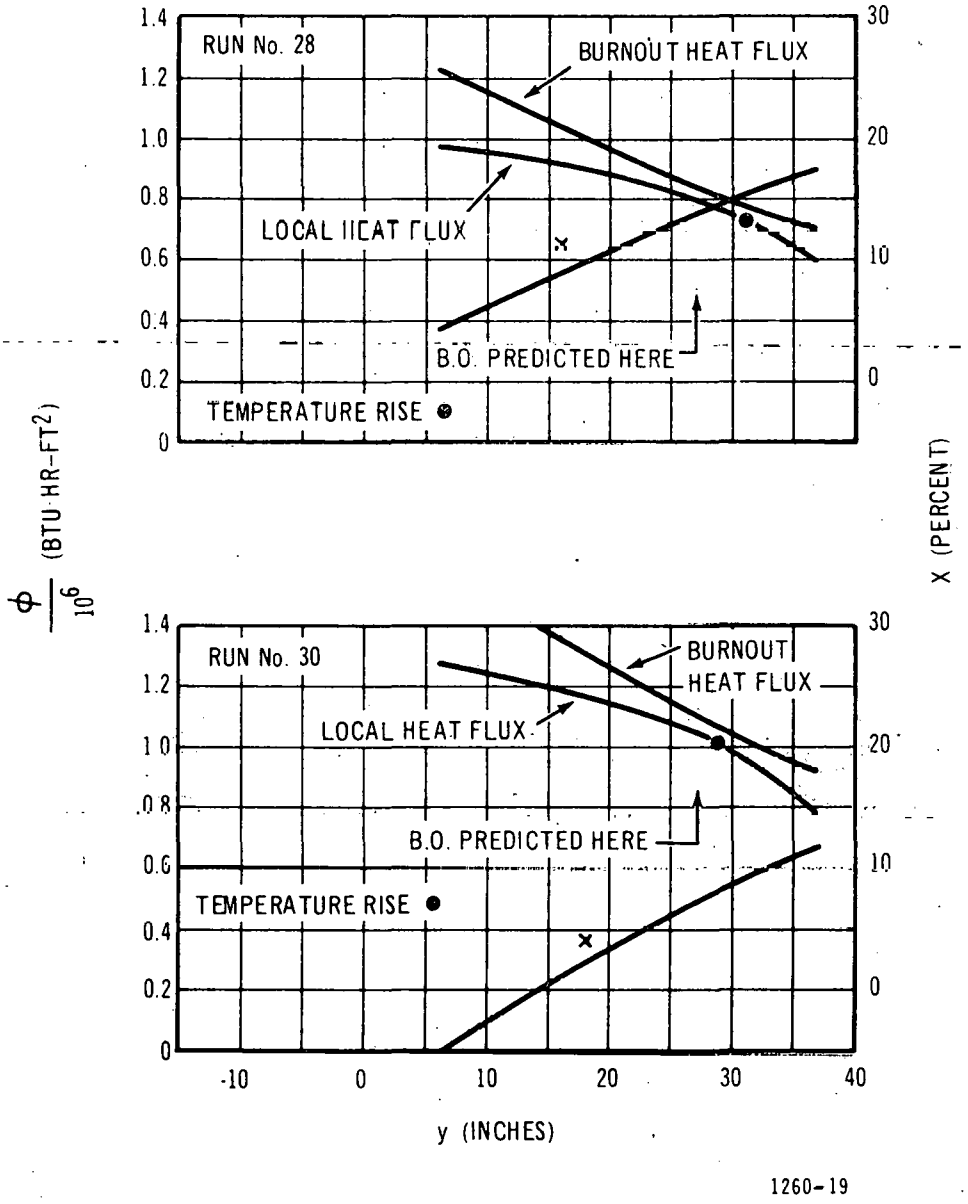

Figure 28. Truncated Cosine Rod
$G = 1.40 \times 10^6$ lb/hr-ft^2

ACKNOWLEDGMENTS

The work reported here was done as part of Task B of the Fuel Cycle Program, sponsored by the U. S. Atomic Energy Commission.

Dr. S. Levy gave help and encouragement in planning the tests and organizing the results. Mr. B. Duncan, and the other people in Building G working under his supervision, set up and conducted the tests, and recorded the data.

APPENDIX

PREDICTION OF BURNOUT FOR A NONUNIFORMLY HEATED ROD

It is postulated for this analysis that the rod is straight, and of constant diameter D_1 along its length. Thermal energy is released in the interior of the rod by unspecified means, such that the heat flux ϕ at the rod surface varies in some specified manner with distance y along the rod, over a length L, and so that $\frac{d\phi}{dy}$ is continuous, but so that ϕ does not vary around the circumference. The average heat flux over the length L is $\bar{\phi}$. Before and after the length L the heat flux is zero.

$$\frac{\phi}{\bar{\phi}} = \psi = f(y), \quad o \leq y \leq L \tag{A-1}$$

$\frac{d\psi}{dy}$ is continuous over $o < y < L$

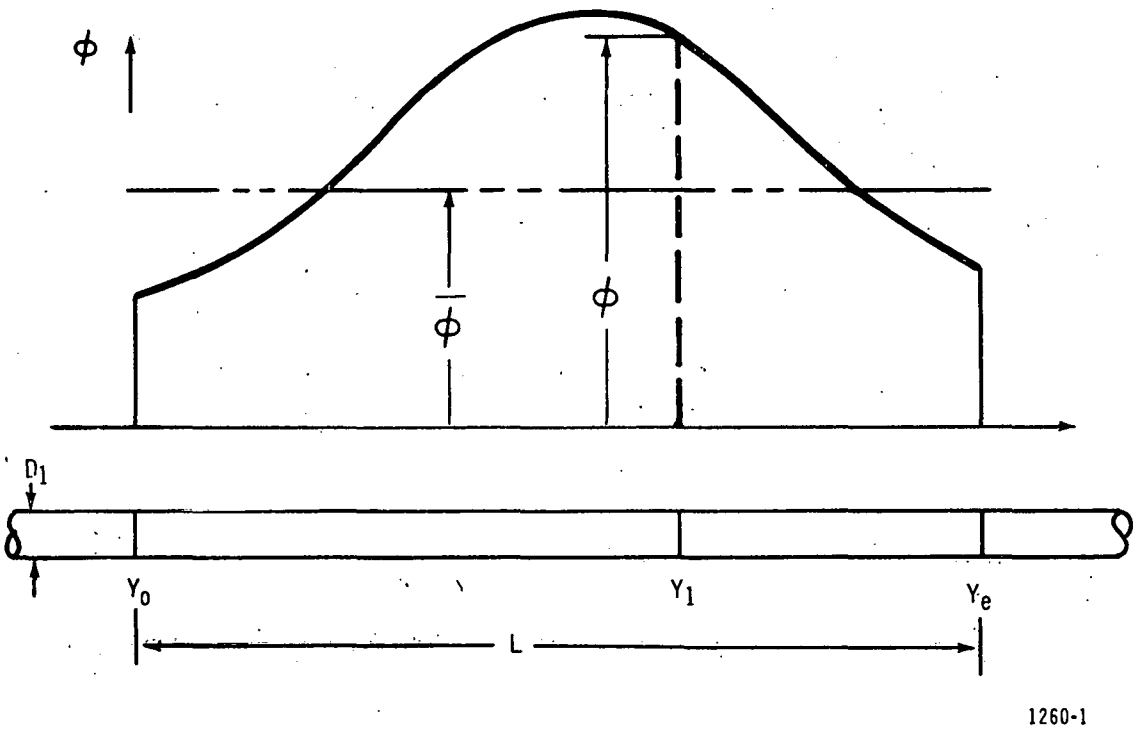

Figure A-1

The rod is inside and parallel with the axis of a vertical tube, so that the coolant flow path between rod and tube is of constant cross section. The cross sectional area of the flow is A. Flow is upward, the coolant enters the bottom of the channel as a liquid with subcooling Δh_s, and leaves the top of the channel at some quality x_e. Except for heat transfer from rod to coolant, the flow is adiabatic. Friction and change in elevation from bottom to top of heated lengths are small enough that the pressure is essentially constant.

It may be noted that the model described above is a close approximation to the cosine rod test conditions.

Referring to Figure A-1, the total heat transfer rate q from $y = y_o$ to $y = y_1$, is

$$q_1 = \int_{y_o}^{y_1} \bar{\phi}\, \pi D_1 dy = \pi D_1 \bar{\phi} \int_{y_o}^{y_1} \psi\, dy = \pi D_1 L \bar{\phi} \left(\frac{r}{R}\right)_1 \qquad \text{(A-2)}$$

The quality at any position y_1 is

$$x_1 = \frac{q_1}{\dot{W} h_{fg}} - \frac{\Delta h_s}{h_{fg}} \qquad \text{(A-3)}$$

It is further postulated that burnout is independent of gradients in the heat flux, and depends only on local quality, geometry, and flow. Per this postulate, the local heat flux at burnout is the same as for a uniformly heated rod.

$$\phi_{bo} = A - Bx \qquad \text{(A-4)}$$

If at any position along the rod $\phi = \phi_{bo}$, then a burnout condition exists.

Let the power, i.e., $\bar{\phi}$, be gradually increased until a burnout condition does in fact exist, at some position y_1. The condition may be represented graphically (see Figure 7).

At $y = y_1$ the following relationships hold:

$$\phi_1 = \phi_{bo} \qquad \text{(A-5)}$$

$$\left(\frac{d\phi}{dy}\right)_1 = \left(\frac{d\phi_{bo}}{dy}\right)_1 \qquad \text{(A-6)}$$

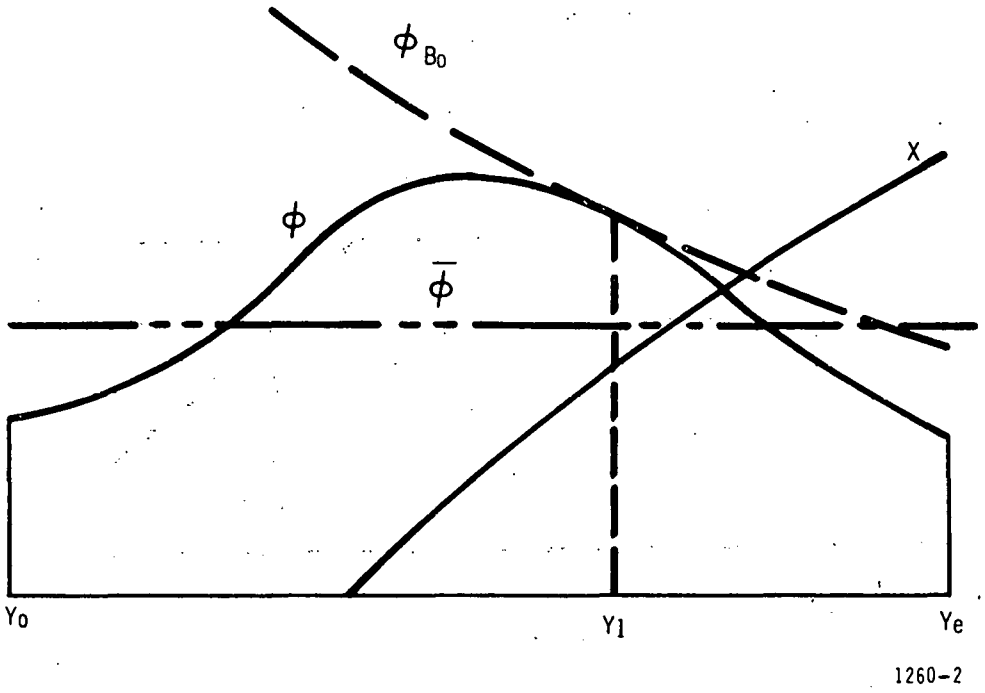

Figure A-2

Combining (A-1), (A-2), (A-3), (A-4), and (A-5):

$$\psi_1 = \frac{1}{\bar{\phi}_{bo}} \left[A + B \frac{\Delta h_s}{h_{fg}} \right] - \frac{B \pi D_1}{\dot{W} h_{fg}} \int_{y_o}^{y_1} \psi \, dy \qquad \text{(A-7)}$$

Differentiating both sides of (A-7) per equation (A-6):

$$\left(\frac{d\psi}{dy} \right) = - \frac{B \pi D_1}{\dot{W} h_{fg}} \psi_1 \qquad \text{(A-8)}$$

or

$$\left(\frac{d \ln \psi}{dy} \right)_1 = - \frac{B \pi D_1}{\dot{W} h_{fg}} \qquad \text{(A-8a)}$$

Both equations (A-7) and (A-8) must be satisfied at burnout. First let us consider equation (A-8). Burnout occurs where the slope is negative, and hence must always occur past the peak value for ψ. If $\frac{d \ln \psi}{dy}$ decreases monotonically past the peak, there is a single solution to equation (A-8), which determines uniquely the location of burnout.

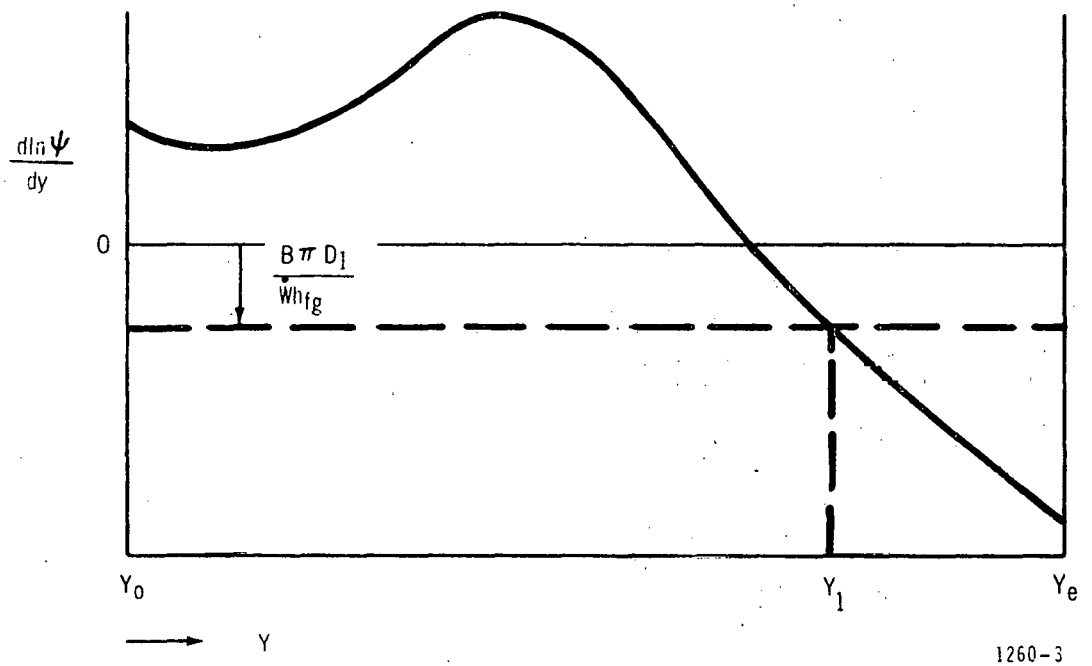

Figure A-3

The location of burnout so determined is independent of power level $\bar{\phi}$ and inlet subcooling Δh_s. Hence, for a given geometry, pressure, and flow, the location is invariant. Note also that for a given geometry and pressure, the constant $\frac{B\pi D_1}{\dot{W}h_{fg}}$ depends only on flow. Hence, there can be a family of solutions which are only flow dependent.

Noting that $\int_{y_o}^{y_1} \psi\, dy = L\left(\frac{r}{R}\right)_1$ and combining (A-1), (A-4), and (A-7),

$$\phi_{bo} = A + B\frac{\Delta h_s}{h_{fg}} - \frac{B\pi D_1}{\dot{W}h_{fg}}\frac{\phi_{bo}}{\psi_1}L\left(\frac{r}{R}\right)_1 \qquad \text{(A-9)}$$

when $\left(\frac{r}{R}\right)_1$ and ψ_1 are functions of y_1, given respectively in Table 1 and in Figures 2A and 2B.

Rearranging,

$$\phi_{bo} = \frac{A + B\dfrac{\Delta h_s}{h_{fg}}}{1 + \dfrac{B\pi D_1 L}{\dot{W} h_{fg}} \dfrac{(r/R)_1}{\psi_1}} \tag{A-10}$$

Thus, the heat flux at burnout is a function of position y_1, determined from equation (A-8); the constants for the burnout curve, equation (A-4); and the inlet subcooling Δh_s. For a given geometry, pressure, and flow, ϕ_{bo} varies linearly with the subcooling.

The average power is simply

$$\bar{\phi}_{bo} = \frac{\phi_{bo}}{\psi_1} \tag{A-11}$$

The quality at burnout is given by

$$x_1 = \frac{1}{h_{fg}} \left[\frac{\bar{\phi}_{bo}\, \pi D_1 L}{\dot{W}} \left(\frac{r}{R} \right)_1 - \Delta h_s \right] \tag{A-12}$$

If it should happen that

$$\frac{d \ln \psi}{dy} > - \frac{B\pi D_1}{\dot{W} h_{fg}} \quad \text{at } y = y_e,$$ then the location of burnout may be at $y = y_e$, i.e., at the exit end of the rod. If this is so, then quality at burnout is x_e, and the heat flux at burnout can be determined by letting $(r/R)_1 = 1$ and $\psi = \psi_e$ in equation (A-10).

If there is more than one predicted position for burnout, then the position which results in the lowest value for predicted average heat flux is the correct position.

NOMENCLATURE

A	=	Channel area, ft^2
A_o	=	Orifice area, ft^2
A	=	Constant
B	=	Constant
B	=	$\left(\frac{D_2}{D_1}\right)^{0.5} (D_2 - D_1)^{-0.2}$
D_o	=	Orifice diameter, ft
D_1	=	Rod diameter, inches or ft
D_2	=	Tube diameter, inches or ft
D_h	=	Hydraulic diameter, inches
g	=	32.17 ft/sec^2
G	=	Mass velocity, $lb/hr\text{-}ft^2$
Δh	=	Manometer deflection, inches
h_1	=	Coolant enthalpy at inlet, Btu/lb
h_f	=	Saturated liquid enthalpy, Btu/lb
Δh_s	=	$h_f - h_1$
h_{fg}	=	Latent heat of vaporization, Btu/lb
k	=	Orifice coefficient
L	=	Heated length, inches
N_{Ro}	=	Orifice Reynolds number
P	=	Pressure
q	=	Total heat transfer rate, Btu/sec
r	=	Electrical resistance of rod from inlet to position y, ohms
R	=	Total electrical resistance of rod, ohms
T_1	=	Temperature at test section inlet, °F
T_{13}	=	Temperature at orifice, °F
T_r	=	Room temperature, °F
w	=	Density of liquid in loop, lb/ft^3
w_r	=	Density of water at room temperature and loop pressure, lb/ft^3
w_{man}	=	Density of manometer fluid, lb/ft^3
$\dot{W}$	=	Flow rate, lb/sec
x	=	Quality = (steam flow rate) ÷ (total flow rate)
x_e	=	Quality at exit end of rod
y	=	Axial coordinate, positive in direction of flow, inches
y_o	=	Inlet end of heated length, inches
y_1	=	Position of burnout, inches
y_e	=	Exit end of heated length, inches
α	=	Linear coefficient of expansion for 304 stainless steel, $°F^{-1}$

μ = Viscosity, $\frac{\text{lb}}{\text{hr-ft}}$

ϕ = Heat flux, Btu/hr-ft^2

$\bar{\phi}$ = Average heat flux, Btu/hr-ft^2

ϕ_{bo} = Burnout heat flux, Btu/hr-ft^2

$\phi_{bo(c)}$ = Burnout heat flux, from uniform rod correlation

$\bar{\phi}_{bo}$ = Average heat flux at burnout

$\bar{\phi}_{bo(p)}$ = Predicted average heat flux at burnout

ψ = $\frac{dr/dy}{R/L} = \phi/\bar{\phi}$, relative heat flux

REFERENCES

1. DeBortoli, R. A., Roarty, J. D., and Weiss, A., "Additional Burnout Data for a Rectangular Channel Having a Cosine Axial Heat Flux", WAPD-TH-227, August 23, 1956.

2. Weiss, A., "Hot Patch Tests in a 0.097 Inch × 1 Inch × 27 Inch Long Rectangular Channel at 2000 psia", WAPD-TH-338, August 7, 1957.

3. Galson, A. F., and Polomik, E. E., "Burnout Data Applicable to Boiling Water Reactors", Paper presented at ANS Pittsburgh Meeting, June 6, 1957.

4. Styrikovich, M. A., Miropol'skii, Z. L., and Chzhao-Yuan Shen, "Effect of Nonuniformity of Heating Along a Length of Pipe on the Magnitude of Critical Heat Fluxes", AEC-TR-4961, Doklady Akad Nauk SSSR 139, No. 4, 859-862 (1961).

5. Swenson, H. S., Carver, J. R., and Kakarala, C. R., "The Influence of Axial Heat Flux Distribution on the Departure from Nuclear Boiling in a Water-Cooled Tube", ASME Paper No. 62-WA-297.

6. Janssen, E., and Kervinen, J. A., "Burnout Conditions for Single Rod in Annular Geometry, Water at 600 to 1400 psia", GEAP-3899, February 1963.

7. DeBortoli, R. A., Green, S. J., LeTourneau, B. W., Troy, M., Weiss, A., "Forced Convection Heat Transfer Burnout Studies for Water in Rectangular Channels and Round Tubes at Pressures Above 500 psia", October 1958, WAPD-188

8. Janssen, E., and Levy, S., "Burnout Limit Curves for Boiling Water Reactors", GE-APED-3892, April 14, 1962.

9. Bishop, A. A., Efferding, L. E., and Tong, L. S., "A Review of Heat Transfer and Fluid Flow of Water in the Supercritical Region and During 'Once-Thru' Operation", WCAP-2040, December 1962 (p. 37).

10. Cook, W. H., "Fuel Cycle Program - First Quarterly Report", GEAP-3558, August 1960 - September 1960.

11. Tong, L. S., Currin, H. B., and Thorp II, A. G., "New Correlations Predict DNB Conditions", Nucleonics, V. 21, n. 5, May 1963, 43-47.